出國報告（出國類別：參加研討會）

# 出席Pacific Rim Meeting On Electronchemical and Solid-State Science2016 (2016世界電化學及固態科學研討會-夏威夷) 心得報告

服務機關：國防大學理工學院動力及系統工程學系
姓名職稱：王樂民教授
派赴國家：美國夏威夷
出國期間：105/10/1~105/10/11
報告日期：105/11/10

**摘要**

世界電化學及固態科學研討會 (Pacific Rim Meeting On Electronchemical and Solid-State Science 2016)為國際間重要會議，每四年於夏威夷舉行一次，如主辦單位宣稱，是世界上最大型極為重要的研討會，會議摘要歷經審查機制才通知是否接受及邀請海報論文發表或口頭發表。

此會議參與學者遍及世界各國，學者研究範圍極廣，學術討論分為：

A.電池及能源科技,B.碳化物奈米結構 C.氧化物及腐蝕特性 D.光電(Photovoltaics)E.電漿奈米科技及技術，磁性材料製程及元件，固-液相介面與電沉積之影響，電沉積在能源技術上的應用

F.工業級電化學應用與工程，電化學創新應用實測研討

G.高純度半導體、半導體、介電材料，金屬在奈米電子上的應用，鍺及相關元件製程，化合物半導體，晶圓接合科技及技術，薄膜電晶體

H.較低次元光電元件，氫化鉀科技，微流體及奈米流體元件，奈米材料及元件

I.燃料電池高分子電解質，固態離子元件，燃料合成反應，水與能源關連(自含鹽的溶液取出動力)，發光即顯示材料基礎及應用

J.固態照明材料

K 生化工程與電化學應用，電化學在有機化學及生物工程近來的應用及面對的問題，物性，分析，電化學催化，光電電化學

L.融化鹽類及離子液體

M.化學感測器，微機電微細製造，奈米材料及元件電化學分析……等，範圍極廣，內容豐碩。

本議程計有 3 場 Plenary Session 報告，5 場 Invited Speakers 報告，上千篇的口頭報告，內容極為豐碩。

本人發表“The effect of Thermal Hydrogenation Processing on the nano-size Grain refinement, mechanical property and corrosion of Ti-6Al-4V alloy”以調整儲氫吸收量的參數來評估及了解形成奈米晶粒的可能機制，並探討其機械性能及耐蝕能力。與會學者，評價良好，會後收到會議主席來謝函表示感謝貢獻該研討會之努力。經與國際間專家研討，對未來研究方向精進，極有助益。近日也收到與此研討會需投稿之 ECS transaction 主編來函正面評價此論文，只要稍作微小修正，即能獲刊登於該期刊，更感此行收穫良多。

# 目次

## 目的

1.赴美國研討會，發表研究成果。
2.與國際學者進行學術交流。

## 過程

此次研討會於 105 年 10 月 2-7 日假美國夏威夷 Convention center 舉行，計有大會演講論壇、論文報告及論文海報展示及說明等項。此次研討範圍如下:

A.電池及能源科技,B.碳化物奈米結構 C.氧化物及腐蝕特性 D.光電(Photovoltaics)E.電漿奈米科技及技術，磁性材料製程及元件，固-液相介面與電沉積之影響，電沉積在能源技術上的應用
F.工業級電化學應用與工程，電化學創新應用實測研討
G.高純度半導體、半導體、介電材料，金屬在奈米電子上的應用，鍺及相關元件製程，化合物半導體，晶圓接合科技及技術，薄膜電晶體
H.較低次元光電元件，氫化鉀科技，微流體及奈米流體元件，奈米材料及元件
I.燃料電池高分子電解質，固態離子元件，燃料合成反應，水與能源關連(自含鹽的溶液取出動力)，發光即顯示材料基礎及應用
J.固態照明材料
K 生化工程與電化學應用，電化學在有機化學及生物工程近來的應用及面對的問題，物性，分析，電化學催化，光電電化學
L.融化鹽類及離子液體
M.化學感測器，微機電微細製造，奈米材料及元件電化學分析……等

10 月 1 日開始接受與會人員報到及論文海報展示備便。10 月 2 日 16:00 為大會開幕式，8:05 時起由大會邀請之 Dr.R.KDixton,美國能源部門主管就 DOE’ s Effects to accelerate the Federally-Funded Technology to the marketplace 進行開場，開始一連串大會及分組議題報告，依大會規劃之場地就各議題實施分組報告與意見交流，最後大會於 10 月 7 日 1700 時舉行圓滿閉幕。

本人獲得邀請之論文口頭報告，大會安排於 10 月 5 日 1200-1220 時，由 Section chair, Prof .Kazuhisa Azumi 主持，此講壇演講主題為“Oxide Formation and Applications”,進行“The effect of Thermal Hydrogenation Processing on the nano-size Grain refinement, mechanical property and corrosion of Ti-6Al-4V alloy”論文口頭報告，(附件一)。嘗試以 Ti-6Al-4V 合金經由先前熱置氫製程調整吸氣量為參數，長出之奈米晶粒的機制進行深入探討，以期未來更能掌握長在此奈米晶粒上的氧化層；並探討其耐蝕性能，及不同吸氣參數下的機械性質。研究結果顯示奈米晶粒形成機制被提出，與會學者及主持人也認同此一新結果，對腐蝕性能影響，機械性質也符預期。報告結束獲與會學者及主持人積極提問並獲滿意答覆。其中所提問題概分為：
(1)為何會想到利用此方法？
(2)差排環是如何產生?
(3)ill-designed area 的觀察與 amorphous 有何不同 ?
(4)即是奈米晶粒、硬度表現如何?
本人逐一回答並解釋，或提問人表達同意，互動良好;會後回台灣後收到會議主席來謝函表示感謝貢獻該研討會之努力。經與國際間專家研討，對未來研究方向精進，極有助益。近日也收到與此研討會需投稿之 ECS transaction 主編來函正面評價此論文，只要稍作微小修正，即能獲刊登於該期刊，更感此行收穫良多。

## 心得及建議

經過此次研討會，看到國際間研發大量投入能源領域，令人印象深刻。在大會會場，更看到各項先進的研究及量測設備技術與展示，也深感國際間競爭與日俱增，我國必須投入相當的研究經費及資源以使國家具競爭力。

經過此次四年一次的國際研討會，深覺教學研究的責任重大，每出國乙次，更覺責任重大。

看到國外學者及對岸中國大陸的研究成果，國內在研究主題上實應集中有效火力，分析最有利我國的大方向，全力推行之。對材料科技之掌握，實應繼續戮力以赴，一定要大量投入資源提升研究能力，掌握製程技術，以電腦技術模擬，精進製程，結合微觀結構分析以改進其機械性質是為必走之方向，更可提升材料性能。目前由於 Ti 合金可投入航空，國防工業及生醫等重要工業，且可結合節能省碳因應潮流及工業需求；亦感我國學人及產學可投入更多能力、經費，使具有國際競爭力，國內相關產業及研究方向亦應朝材料科學減重強化發展。

將來學生也與世界接軌，未來更當於學生報告中，半強迫及鼓勵其以英文報告，撰寫研究成果提升英文能力。

# 附件一　本人受邀發表論文簡報

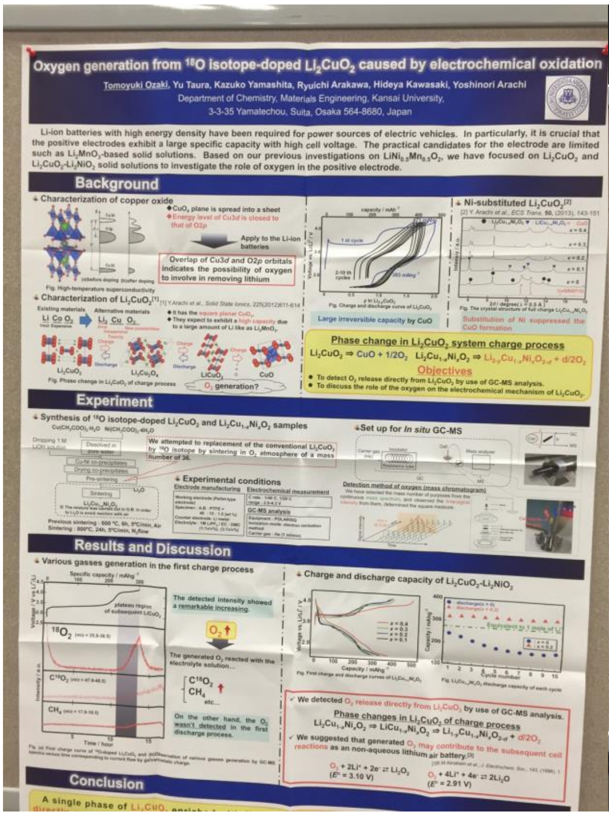


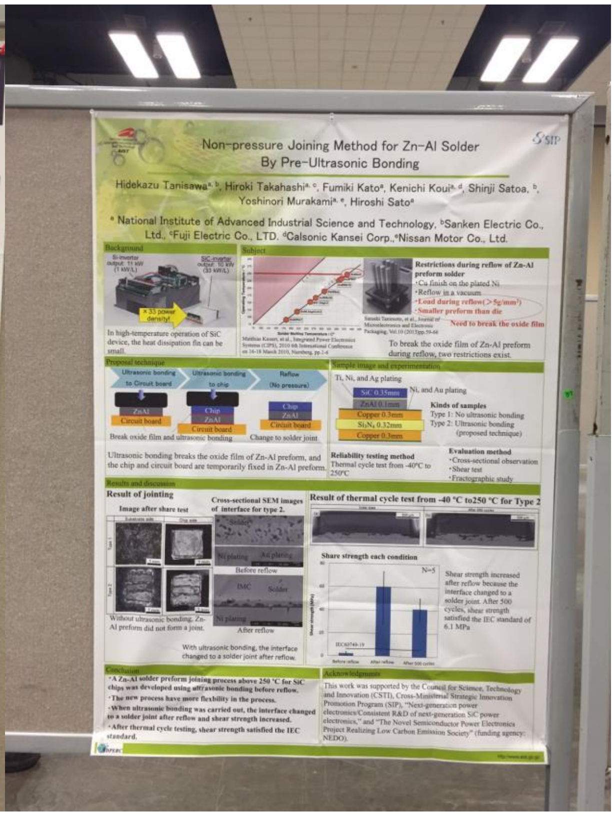


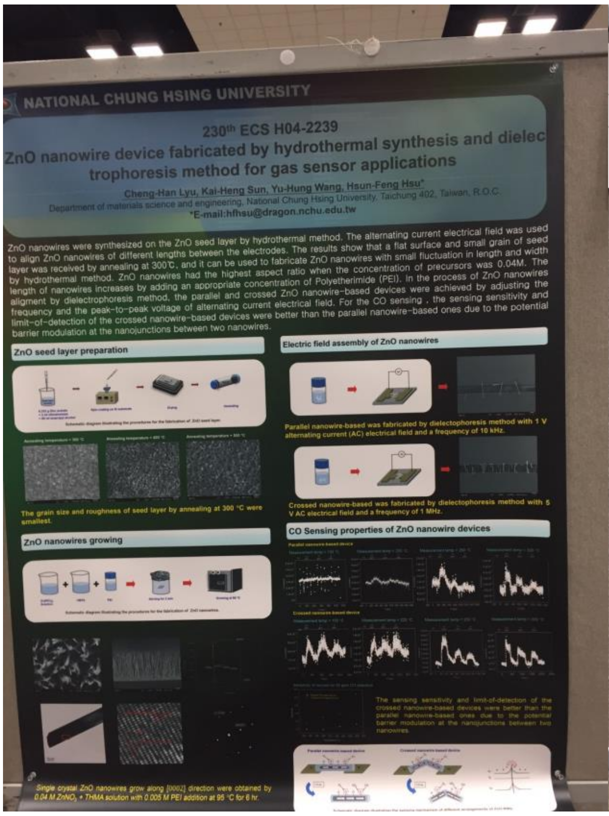


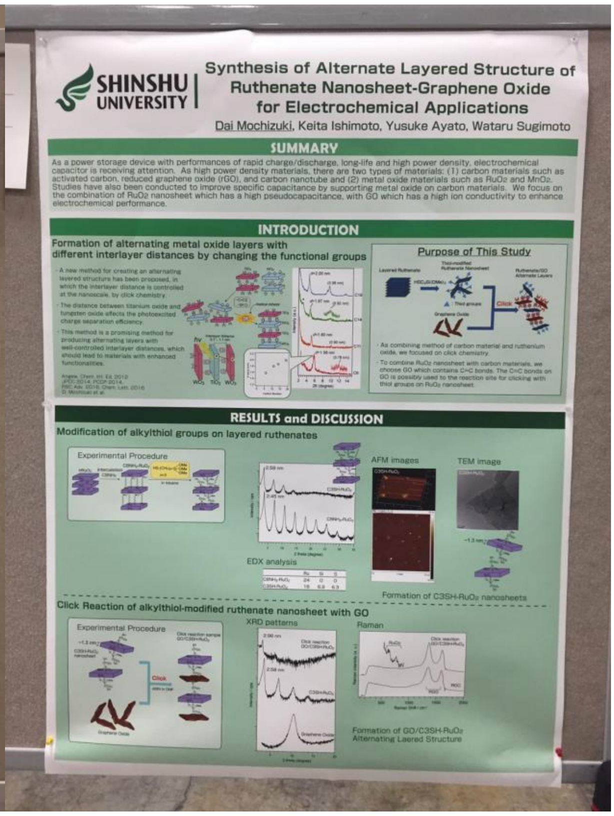

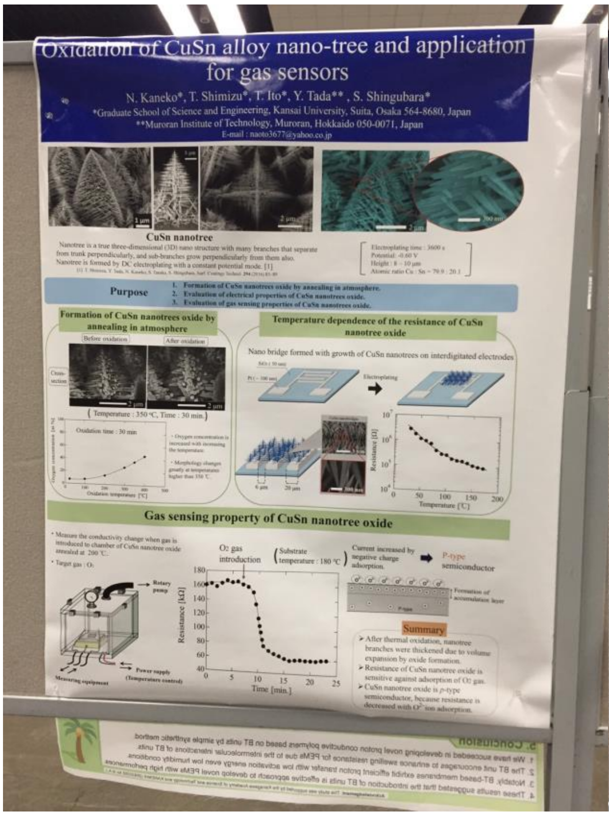
Oxidation of CuSn alloy nano-tree and application for gas sensors
N. Kaneko*, T. Shimizu*, T. Ito*, Y. Tada**, S. Shingubara*
*Graduate School of Science and Engineering, Kansai University, Suita, Osaka 564-8680, Japan
**Muroran Institute of Technology, Muroran, Hokkaido 050-0071, Japan
CuSn nanotree
Purpose
Formation of CuSn nanotrees oxide by annealing in atmosphere
Temperature dependence of the resistance of CuSn nanotree oxide
Gas sensing property of CuSn nanotree oxide
Summary
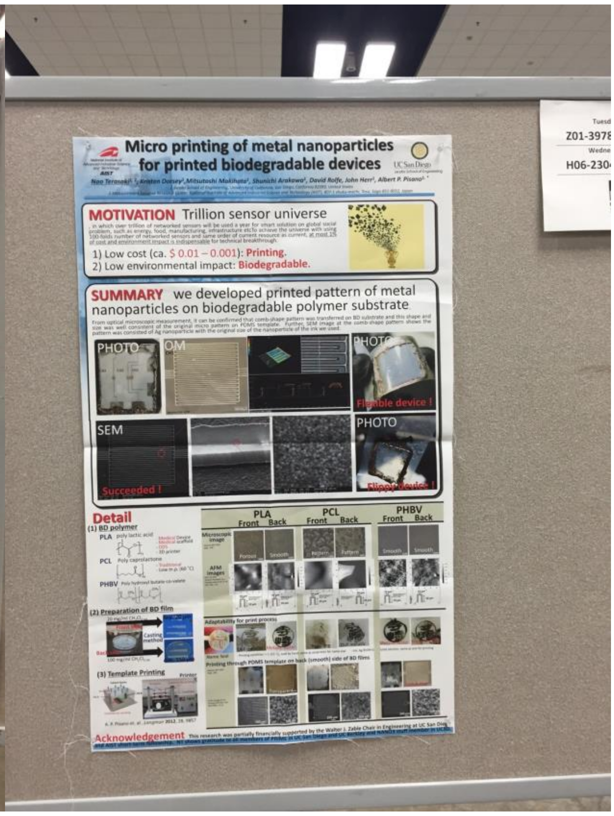
Micro printing of metal nanoparticles for printed biodegradable devices
MOTIVATION Trillion sensor universe
1) Low cost (ca. $ 0.01 – 0.001): Printing.
2) Low environmental impact: Biodegradable.
SUMMARY we developed printed pattern of metal nanoparticles on biodegradable polymer substrate
PHOTO
OM
SEM
Flexible device !
Succeeded !
Detail
PLA
PCL
PHBV
Acknowledgement
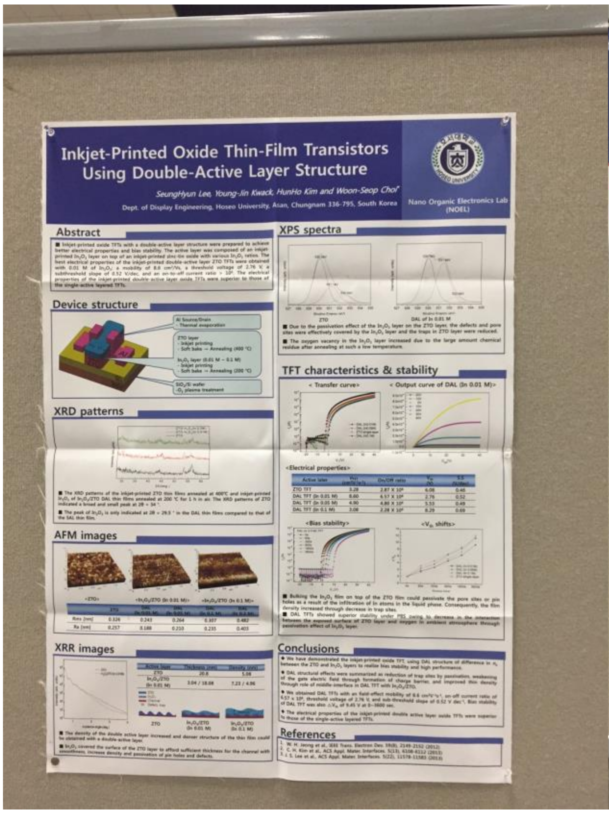
Inkjet-Printed Oxide Thin-Film Transistors Using Double-Active Layer Structure
SeungHyun Lee, Young-Jin Kwack, HunHo Kim and Woon-Seop Choi
Dept. of Display Engineering, Hoseo University, Asan, Chungnam 336-795, South Korea
Nano Organic Electronics Lab (NOEL)
Abstract
XPS spectra
Device structure
TFT characteristics & stability
XRD patterns
AFM images
XRR images
Conclusions
References
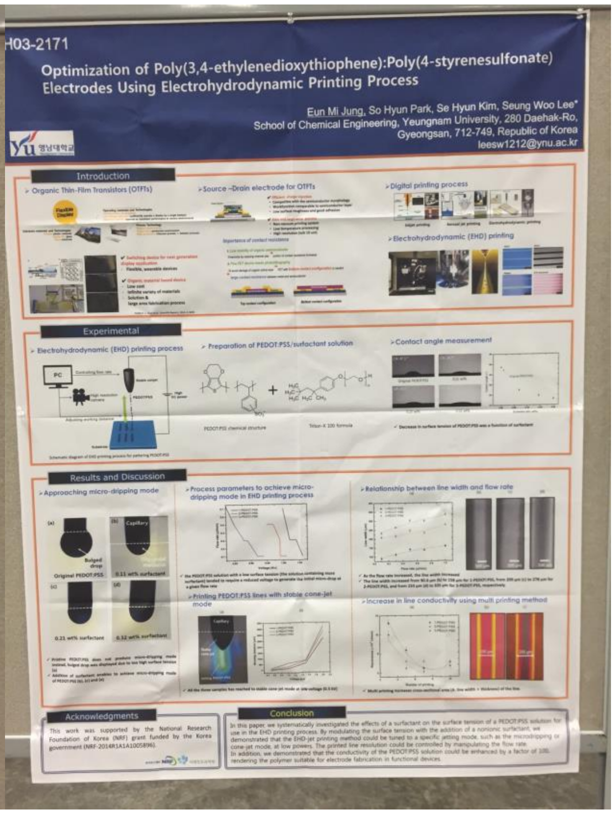
H03-2171
Optimization of Poly(3,4-ethylenedioxythiophene):Poly(4-styrenesulfonate) Electrodes Using Electrohydrodynamic Printing Process
Eun Mi Jung, So Hyun Park, Se Hyun Kim, Seung Woo Lee*
School of Chemical Engineering, Yeungnam University, 280 Daehak-Ro, Gyeongsan, 712-749, Republic of Korea
leesw1212@ynu.ac.kr
Introduction
Experimental
Results and Discussion
Acknowledgments
Conclusion

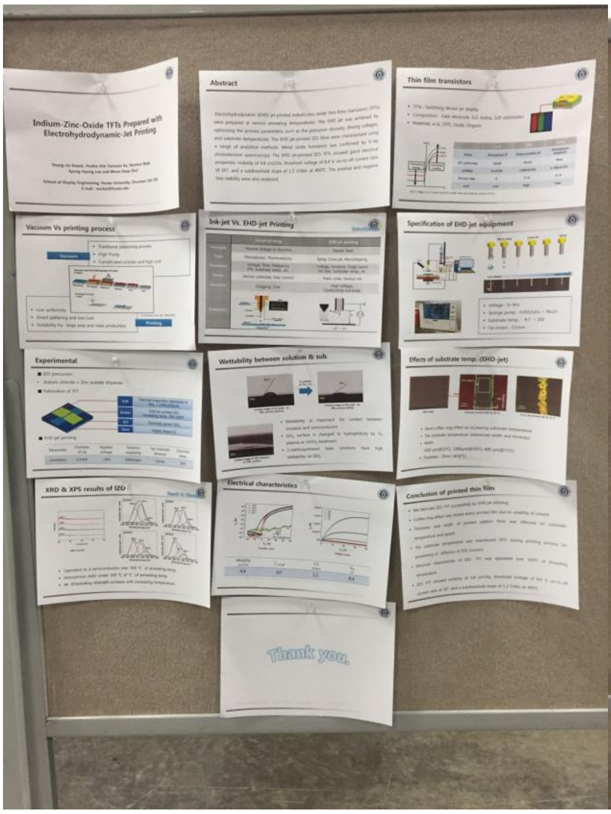
Indium-Zinc-Oxide TFTs Prepared with Electrohydrodynamic-Jet Printing
Abstract
Thin film transistors
Vacuum Vs printing process
Ink-jet Vs. EHD-jet Printing
Specification of EHD-jet equipment
Experimental
Wettability between solution & sub.
Effects of substrate temp. (EHD-jet)
XRD & XPS results of IZO
Electrical characteristics
Conclusion of printed thin film
Thank you.

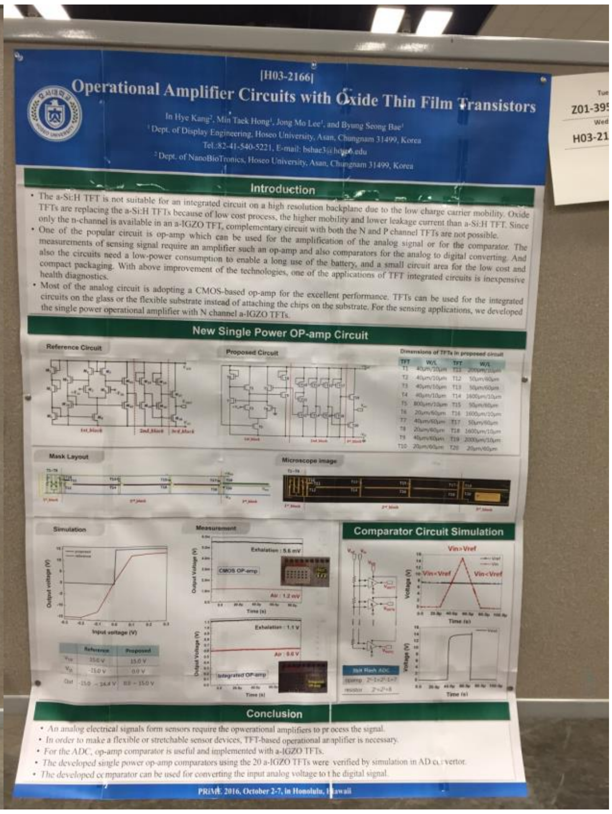
[H03-2166]
Operational Amplifier Circuits with Oxide Thin Film Transistors
Introduction
New Single Power OP-amp Circuit
Reference Circuit
Proposed Circuit
Mask Layout
Microscope image
Simulation
Measurement
Comparator Circuit Simulation
Conclusion
PRiME 2016, October 2-7, in Honolulu, Hawaii

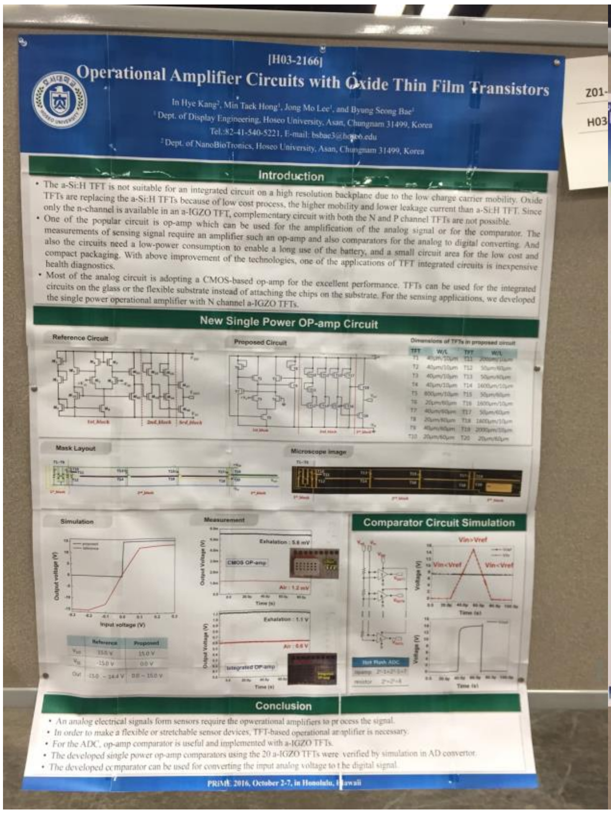
[H03-2166]
Operational Amplifier Circuits with Oxide Thin Film Transistors
Introduction
New Single Power OP-amp Circuit
Reference Circuit
Proposed Circuit
Mask Layout
Microscope image
Simulation
Measurement
Comparator Circuit Simulation
Conclusion
PRiME 2016, October 2-7, in Honolulu, Hawaii

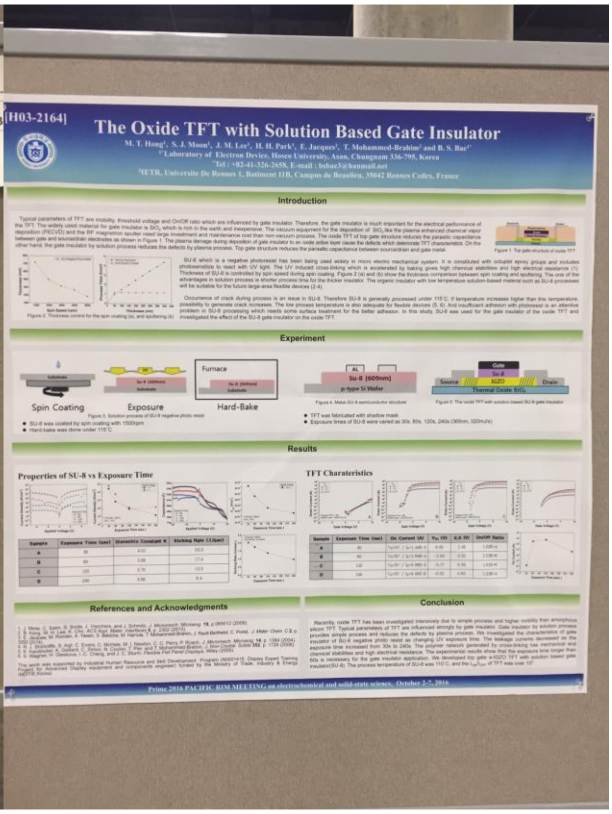
[H03-2164]
The Oxide TFT with Solution Based Gate Insulator
Introduction
Experiment
Spin Coating
Exposure
Hard-Bake
Results
Properties of SU-8 vs Exposure Time
TFT Charateristics
References and Acknowledgments
Conclusion

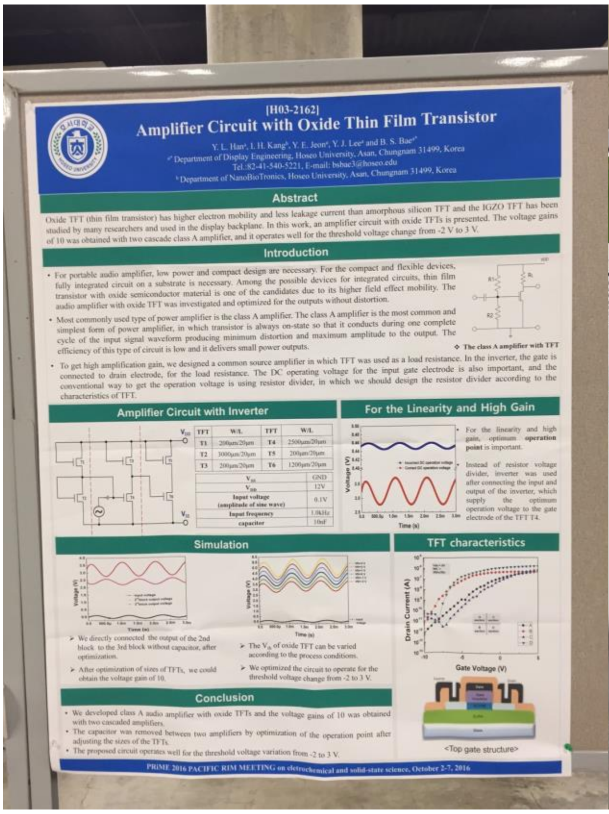
[H03-2162]
Amplifier Circuit with Oxide Thin Film Transistor
Y. L. Han, J. H. Kang, Y. E. Jeon, Y. J. Lee and B. S. Bae
Department of Display Engineering, Hoseo University, Asan, Chungnam 31499, Korea
Department of NanoBioTronics, Hoseo University, Asan, Chungnam 31499, Korea
Abstract
Introduction
Amplifier Circuit with Inverter
For the Linearity and High Gain
Simulation
TFT characteristics
Conclusion
PRiME 2016 PACIFIC RIM MEETING on electrochemical and solid-state science, October 2-7, 2016

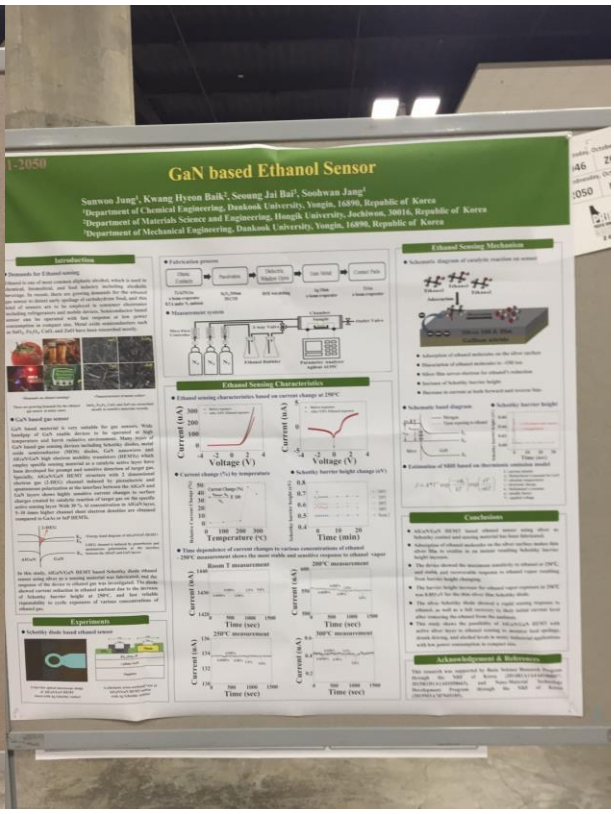
GaN based Ethanol Sensor
Department of Chemical Engineering, Dankook University, Yongin, 16890, Republic of Korea
Department of Materials Science and Engineering, Hongik University, Jochiwon, 30016, Republic of Korea
Department of Mechanical Engineering, Dankook University, Yongin, 16890, Republic of Korea
Introduction
Ethanol Sensing Mechanism
Ethanol Sensing Characteristics
Experiments
Conclusions
Acknowledgement & References

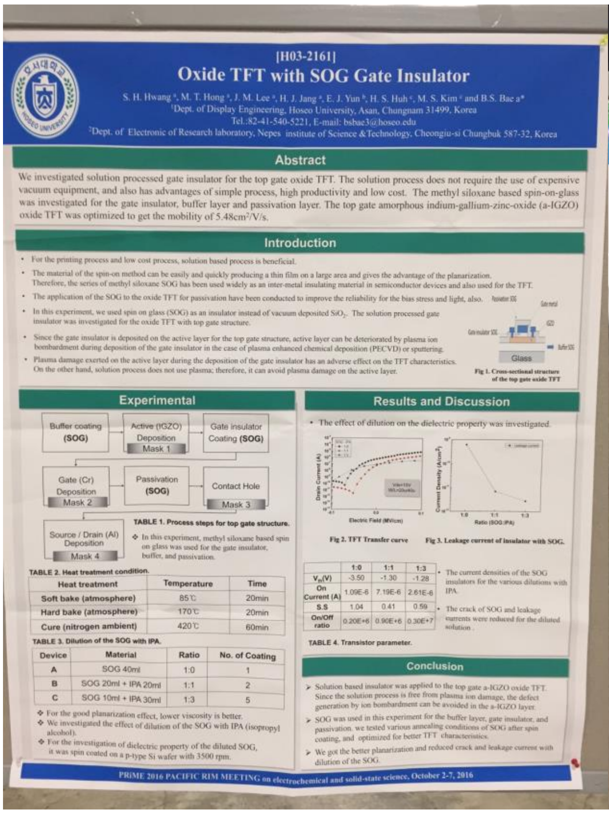
[H03-2161]
Oxide TFT with SOG Gate Insulator
Dept. of Display Engineering, Hoseo University, Asan, Chungnam 31499, Korea
Abstract
Introduction
Experimental
Results and Discussion
Conclusion
PRiME 2016 PACIFIC RIM MEETING on electrochemical and solid-state science, October 2-7, 2016

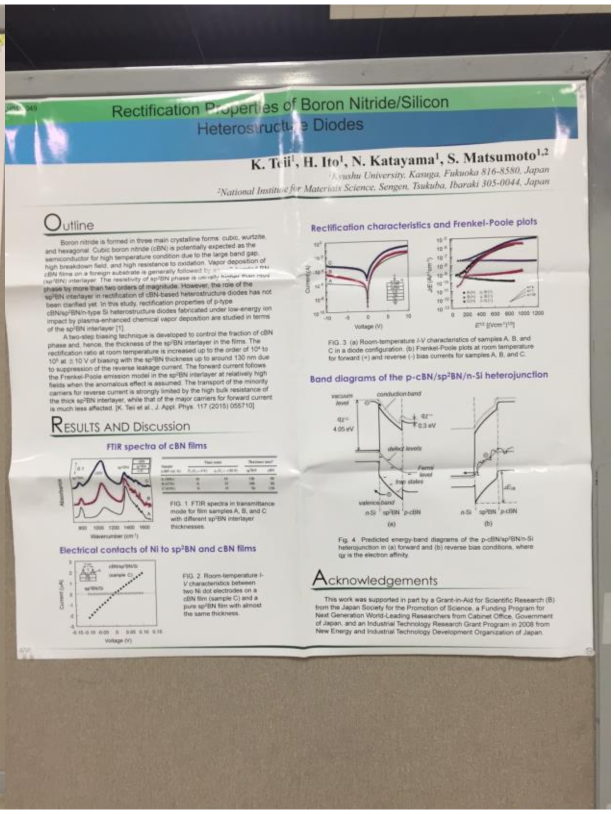
Rectification Properties of Boron Nitride/Silicon Heterostructure Diodes
K. Teii, H. Ito, N. Katayama, S. Matsumoto
Kyushu University, Kasuga, Fukuoka 816-8580, Japan
National Institute for Materials Science, Sengen, Tsukuba, Ibaraki 305-0044, Japan
Outline
Rectification characteristics and Frenkel-Poole plots
Band diagrams of the p-cBN/sp2BN/n-Si heterojunction
Results and Discussion
FTIR spectra of cBN films
Electrical contacts of Ni to sp2BN and cBN films
Acknowledgements

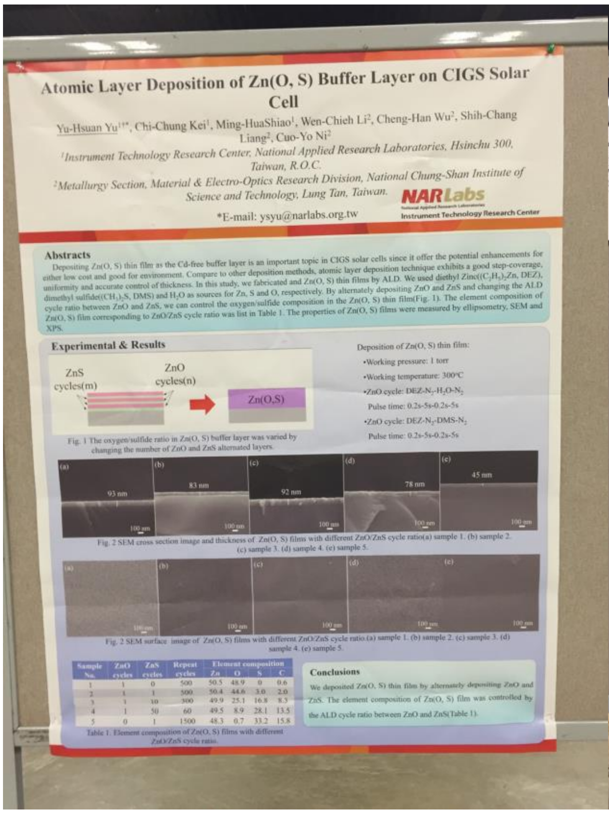
Atomic Layer Deposition of Zn(O, S) Buffer Layer on CIGS Solar Cell
Yu-Hsuan Yu, Chi-Chung Kei, Ming-HuaShiao, Wen-Chieh Li, Cheng-Han Wu, Shih-Chang Liang, Cuo-Yo Ni
Instrument Technology Research Center, National Applied Research Laboratories, Hsinchu 300, Taiwan, R.O.C.
Metallurgy Section, Material & Electro-Optics Research Division, National Chung-Shan Institute of Science and Technology, Lung Tan, Taiwan.
NARLabs
*E-mail: ysyu@narlabs.org.tw
Abstracts
Experimental & Results
ZnS cycles(m)
ZnO cycles(n)
Zn(O,S)
Deposition of Zn(O, S) thin film:
•Working pressure: 1 torr
•Working temperature: 300°C
Fig. 1 The oxygen/sulfide ratio in Zn(O, S) buffer layer was varied by changing the number of ZnO and ZnS alternated layers.
Conclusions

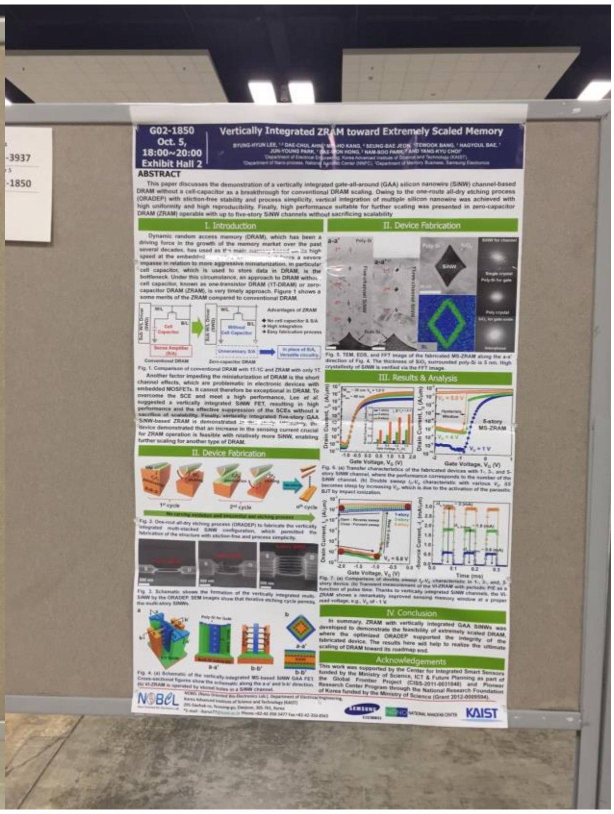
G02-1850
Oct. 5,
18:00~20:00
Exhibit Hall 2
Vertically Integrated ZRAM toward Extremely Scaled Memory
ABSTRACT
I. Introduction
II. Device Fabrication
III. Results & Analysis
IV. Conclusion
Acknowledgements
KAIST

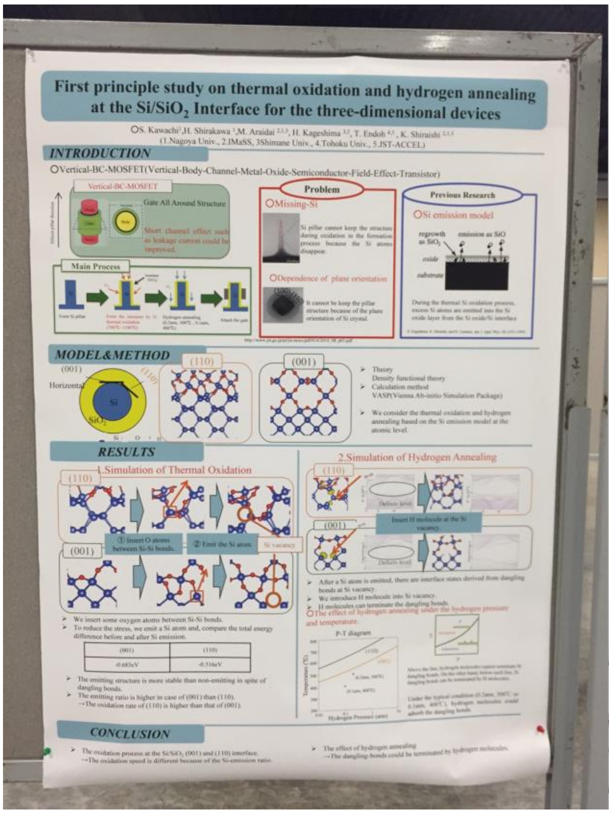
First principle study on thermal oxidation and hydrogen annealing at the Si/SiO2 Interface for the three-dimensional devices
INTRODUCTION
Vertical-BC-MOSFET(Vertical-Body-Channel-Metal-Oxide-Semiconductor-Field-Effect-Transistor)
Problem
Previous Research
Main Process
MODEL&METHOD
RESULTS
1.Simulation of Thermal Oxidation
2.Simulation of Hydrogen Annealing
CONCLUSION

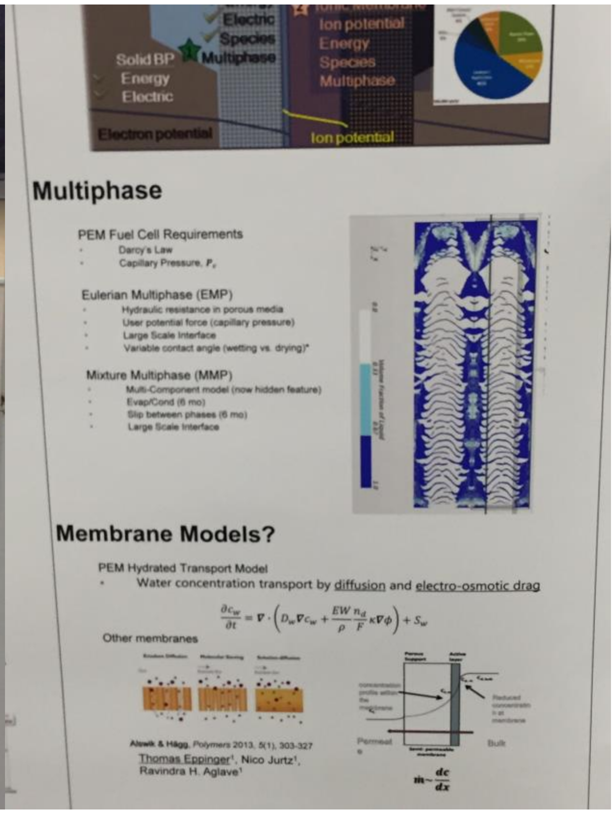
Solid BP
Energy
Electric
Species
Multiphase
Ion potential
Energy
Species
Multiphase
Electron potential
Ion potential
Multiphase
PEM Fuel Cell Requirements
Darcy's Law
Capillary Pressure, $P_c$
Eulerian Multiphase (EMP)
Hydraulic resistance in porous media
User potential force (capillary pressure)
Large Scale Interface
Variable contact angle (wetting vs. drying)*
Mixture Multiphase (MMP)
Multi-Component model (now hidden feature)
Evap/Cond (6 mo)
Slip between phases (6 mo)
Large Scale Interface
Membrane Models?
PEM Hydrated Transport Model
Water concentration transport by diffusion and electro-osmotic drag
$\frac{\partial c_w}{\partial t} = \nabla \cdot \left( D_w \nabla c_w + \frac{EW}{\rho} \frac{n_d}{F} \kappa \nabla \phi \right) + S_w$
Other membranes
Alswik & Hägg, Polymers 2013, 5(1), 303-327
Thomas Eppinger, Nico Jurtz, Ravindra H. Aglave

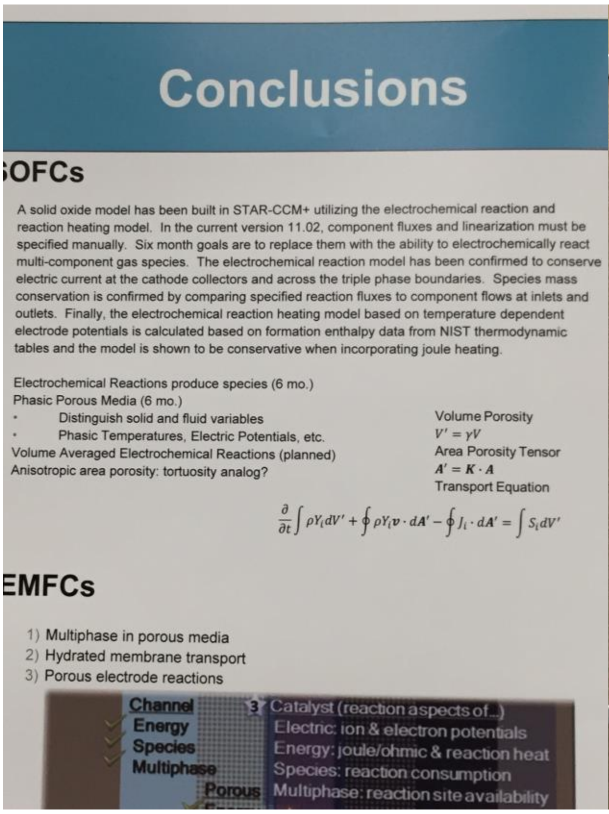
Conclusions
SOFCs
A solid oxide model has been built in STAR-CCM+ utilizing the electrochemical reaction and reaction heating model. In the current version 11.02, component fluxes and linearization must be specified manually. Six month goals are to replace them with the ability to electrochemically react multi-component gas species. The electrochemical reaction model has been confirmed to conserve electric current at the cathode collectors and across the triple phase boundaries. Species mass conservation is confirmed by comparing specified reaction fluxes to component flows at inlets and outlets. Finally, the electrochemical reaction heating model based on temperature dependent electrode potentials is calculated based on formation enthalpy data from NIST thermodynamic tables and the model is shown to be conservative when incorporating joule heating.
Electrochemical Reactions produce species (6 mo.)
Phasic Porous Media (6 mo.)
Distinguish solid and fluid variables
Phasic Temperatures, Electric Potentials, etc.
Volume Averaged Electrochemical Reactions (planned)
Anisotropic area porosity: tortuosity analog?
Volume Porosity
$V' = \gamma V$
Area Porosity Tensor
$A' = K \cdot A$
Transport Equation
$\frac{\partial}{\partial t}\int \rho Y_i dV' + \oint \rho Y_i \boldsymbol{v} \cdot dA' - \oint J_i \cdot dA' = \int S_i dV'$
EMFCs
1) Multiphase in porous media
2) Hydrated membrane transport
3) Porous electrode reactions
Channel
Energy
Species
Multiphase
Porous
3 Catalyst (reaction aspects of...)
Electric: ion & electron potentials
Energy: joule/ohmic & reaction heat
Species: reaction consumption
Multiphase: reaction site availability

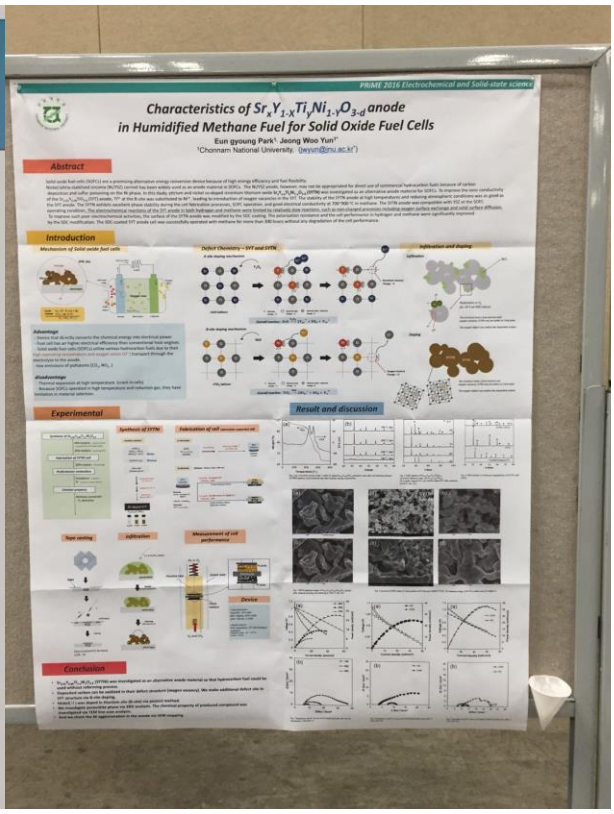
PRiME 2016 Electrochemical and Solid-state science
Characteristics of $Sr_xY_{1-x}Ti_yNi_{1-y}O_{3-d}$ anode in Humidified Methane Fuel for Solid Oxide Fuel Cells
Eun gyoung Park, Jeong Woo Yun
Chonnam National University
Abstract
Introduction
Experimental
Result and discussion
Conclusion

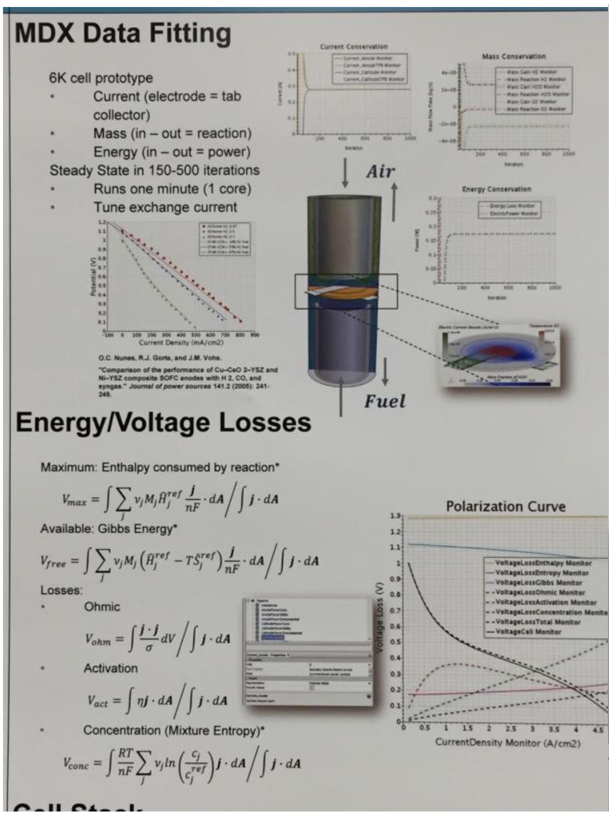
MDX Data Fitting
6K cell prototype
Current (electrode = tab collector)
Mass (in – out = reaction)
Energy (in – out = power)
Steady State in 150-500 iterations
Runs one minute (1 core)
Tune exchange current
Current Conservation
Mass Conservation
Energy Conservation
Air
Fuel
Current Density (mA/cm2)
O.C. Nunes, R.J. Gorte, and J.M. Vohs.
"Comparison of the performance of Cu-CeO 2-YSZ and Ni-YSZ composite SOFC anodes with H 2, CO, and syngas." Journal of power sources 141.2 (2005): 241-249.
Energy/Voltage Losses
Maximum: Enthalpy consumed by reaction*
$V_{max} = \int \sum_j \nu_j M_j \bar{H}_j^{ref} \frac{j}{nF} \cdot dA \Big/ \int j \cdot dA$
Available: Gibbs Energy*
$V_{free} = \int \sum_j \nu_j M_j \left(\bar{H}_j^{ref} - T\bar{S}_j^{ref}\right) \frac{j}{nF} \cdot dA \Big/ \int j \cdot dA$
Losses:
Ohmic
$V_{ohm} = \int \frac{j \cdot j}{\sigma} dV \Big/ \int j \cdot dA$
Activation
$V_{act} = \int \eta j \cdot dA \Big/ \int j \cdot dA$
Concentration (Mixture Entropy)*
$V_{conc} = \int \frac{RT}{nF} \sum_j \nu_j \ln\left(\frac{c_j}{c_j^{ref}}\right) j \cdot dA \Big/ \int j \cdot dA$
Polarization Curve
VoltageLossEnthalpy Monitor
VoltageLossEntropy Monitor
VoltageLossGibbs Monitor
VoltageLossOhmic Monitor
VoltageLossActivation Monitor
VoltageLossConcentration Monitor
VoltageLossTotal Monitor
VoltageCell Monitor
Voltage Loss (V)
CurrentDensity Monitor (A/cm2)

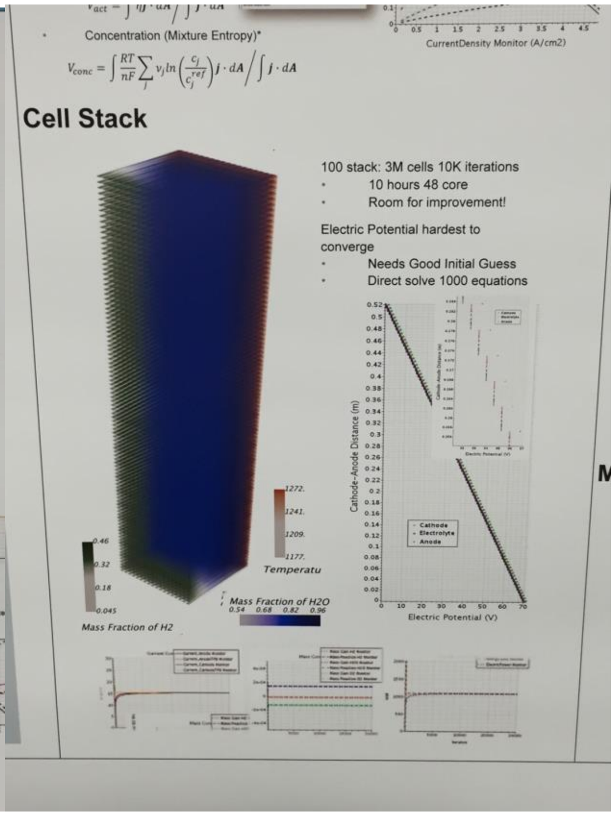
Concentration (Mixture Entropy)*
$V_{conc} = \int \frac{RT}{nF} \sum_j \nu_j \ln\left(\frac{c_j}{c_j^{ref}}\right) j \cdot dA \Big/ \int j \cdot dA$
CurrentDensity Monitor (A/cm2)
Cell Stack
100 stack: 3M cells 10K iterations
10 hours 48 core
Room for improvement!
Electric Potential hardest to converge
Needs Good Initial Guess
Direct solve 1000 equations
Mass Fraction of H2
Mass Fraction of H2O
Temperatu
Cathode-Anode Distance (m)
Electric Potential (V)
Cathode
Electrolyte
Anode

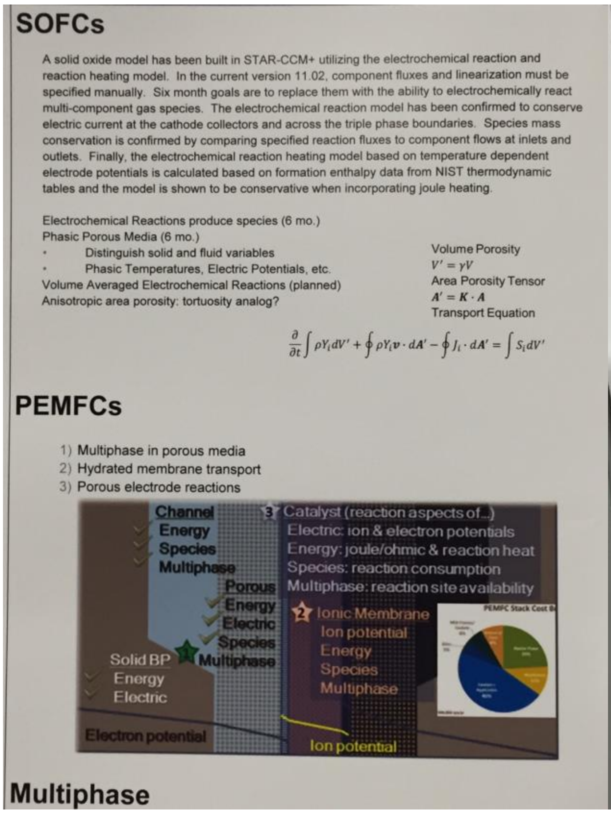
SOFCs
A solid oxide model has been built in STAR-CCM+ utilizing the electrochemical reaction and reaction heating model. In the current version 11.02, component fluxes and linearization must be specified manually. Six month goals are to replace them with the ability to electrochemically react multi-component gas species. The electrochemical reaction model has been confirmed to conserve electric current at the cathode collectors and across the triple phase boundaries. Species mass conservation is confirmed by comparing specified reaction fluxes to component flows at inlets and outlets. Finally, the electrochemical reaction heating model based on temperature dependent electrode potentials is calculated based on formation enthalpy data from NIST thermodynamic tables and the model is shown to be conservative when incorporating joule heating.
Electrochemical Reactions produce species (6 mo.)
Phasic Porous Media (6 mo.)
Distinguish solid and fluid variables
Phasic Temperatures, Electric Potentials, etc.
Volume Averaged Electrochemical Reactions (planned)
Anisotropic area porosity: tortuosity analog?
Volume Porosity
$V' = \gamma V$
Area Porosity Tensor
$A' = K \cdot A$
Transport Equation
$\frac{\partial}{\partial t}\int \rho Y_i dV' + \oint \rho Y_i \mathbf{v} \cdot dA' - \oint J_i \cdot dA' = \int S_i dV'$
PEMFCs
1) Multiphase in porous media
2) Hydrated membrane transport
3) Porous electrode reactions
Channel
Energy
Species
Multiphase
Porous
Energy
Electric
Species
Multiphase
Solid BP
Energy
Electric
3 Catalyst (reaction aspects of...)
Electric: ion & electron potentials
Energy: joule/ohmic & reaction heat
Species: reaction consumption
Multiphase: reaction site availability
2 Ionic Membrane
Ion potential
Energy
Species
Multiphase
PEMFC Stack Cost B
Electron potential
Ion potential
Multiphase

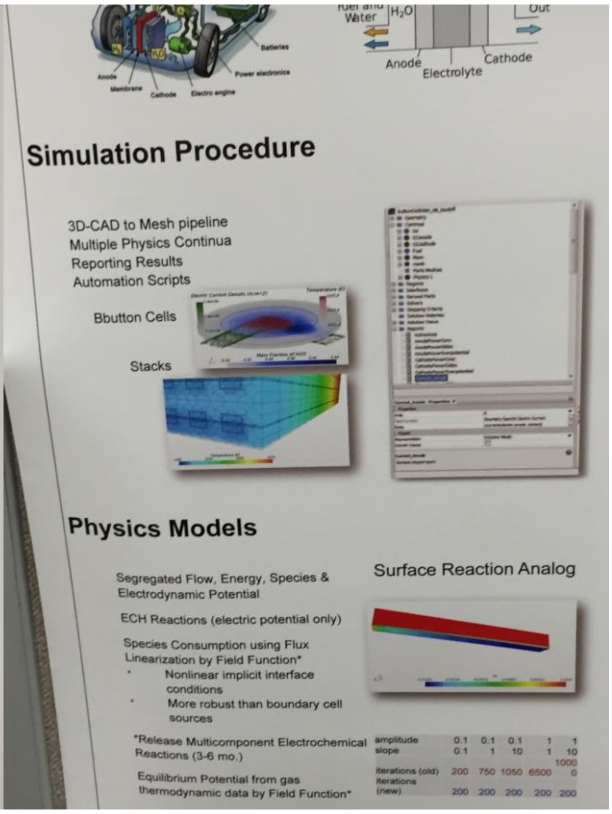
Batteries
Anode
Membrane
Cathode
Electro engine
Power electronics
Water
$H_2O$
Out
Anode
Electrolyte
Cathode
Simulation Procedure
3D-CAD to Mesh pipeline
Multiple Physics Continua
Reporting Results
Automation Scripts
Bbutton Cells
Stacks
Physics Models
Segregated Flow, Energy, Species & Electrodynamic Potential
ECH Reactions (electric potential only)
Species Consumption using Flux Linearization by Field Function*
Nonlinear implicit interface conditions
More robust than boundary cell sources
*Release Multicomponent Electrochemical Reactions (3-6 mo.)
Equilibrium Potential from gas thermodynamic data by Field Function*
Surface Reaction Analog
amplitude 0.1 0.1 0.1 1 1
slope 0.1 1 10 1 10
iterations (old) 200 750 1050 6500 1000 0
iterations (new) 200 200 200 200 200

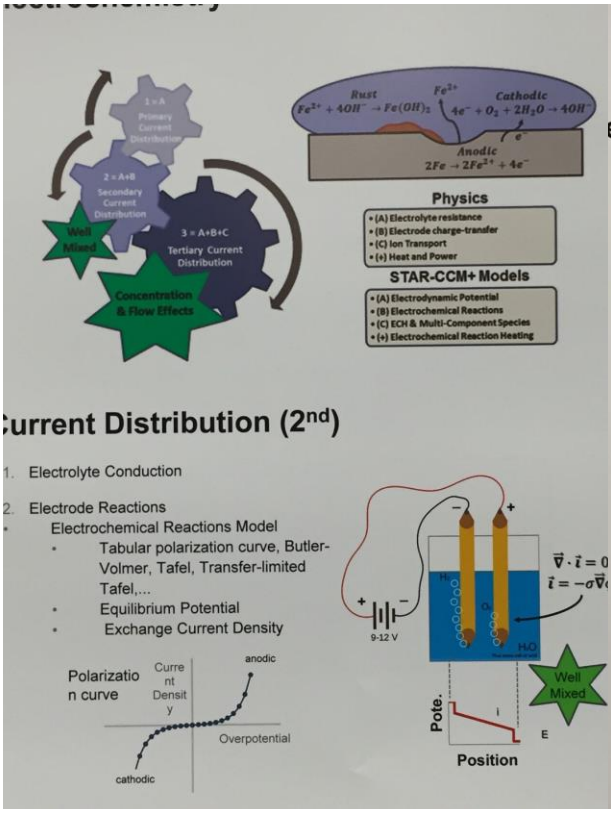
1 = A
Primary Current Distribution
2 = A+B
Secondary Current Distribution
3 = A+B+C
Tertiary Current Distribution
Well Mixed
Concentration & Flow Effects
Rust
$Fe^{2+}$
Cathodic
$Fe^{2+} + 4OH^- \rightarrow Fe(OH)_2$
$4e^- + O_2 + 2H_2O \rightarrow 4OH^-$
Anodic
$2Fe \rightarrow 2Fe^{2+} + 4e^-$
Physics
• (A) Electrolyte resistance
• (B) Electrode charge-transfer
• (C) Ion Transport
• (+) Heat and Power
STAR-CCM+ Models
• (A) Electrodynamic Potential
• (B) Electrochemical Reactions
• (C) ECH & Multi-Component Species
• (+) Electrochemical Reaction Heating
Current Distribution (2nd)
1. Electrolyte Conduction
2. Electrode Reactions
Electrochemical Reactions Model
Tabular polarization curve, Butler-Volmer, Tafel, Transfer-limited Tafel,...
Equilibrium Potential
Exchange Current Density
Polarization curve
Current Density
anodic
cathodic
Overpotential
9-12 V
$H_2$
$O_2$
$H_2O$
$\vec{\nabla} \cdot \vec{i} = 0$
$\vec{i} = -\sigma\vec{\nabla}$
Well Mixed
Pote.
Position
E

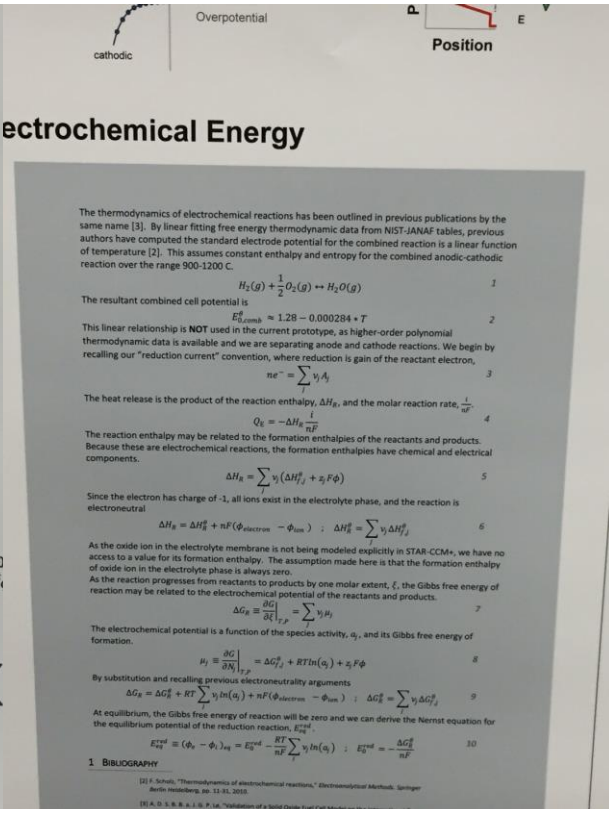
cathodic
Overpotential
Position
ectrochemical Energy
The thermodynamics of electrochemical reactions has been outlined in previous publications by the same name [3]. By linear fitting free energy thermodynamic data from NIST-JANAF tables, previous authors have computed the standard electrode potential for the combined reaction is a linear function of temperature [2]. This assumes constant enthalpy and entropy for the combined anodic-cathodic reaction over the range 900-1200 C.
$H_2(g) + \frac{1}{2}O_2(g) \leftrightarrow H_2O(g)$ 1
The resultant combined cell potential is
$E^{\theta}_{0,comb} \approx 1.28 - 0.000284 \cdot T$ 2
This linear relationship is NOT used in the current prototype, as higher-order polynomial thermodynamic data is available and we are separating anode and cathode reactions. We begin by recalling our "reduction current" convention, where reduction is gain of the reactant electron,
$ne^- = \sum_j \nu_j A_j$ 3
The heat release is the product of the reaction enthalpy, $\Delta H_R$, and the molar reaction rate, $\frac{i}{nF}$.
$Q_E = -\Delta H_R \frac{i}{nF}$ 4
The reaction enthalpy may be related to the formation enthalpies of the reactants and products. Because these are electrochemical reactions, the formation enthalpies have chemical and electrical components.
$\Delta H_R = \sum_j \nu_j (\Delta H^{\theta}_{f,j} + z_j F\phi)$ 5
Since the electron has charge of -1, all ions exist in the electrolyte phase, and the reaction is electroneutral
$\Delta H_R = \Delta H^{\theta}_R + nF(\phi_{electron} - \phi_{ion})\ ;\ \Delta H^{\theta}_R = \sum_j \nu_j \Delta H^{\theta}_{f,j}$ 6
As the oxide ion in the electrolyte membrane is not being modeled explicitly in STAR-CCM+, we have no access to a value for its formation enthalpy. The assumption made here is that the formation enthalpy of oxide ion in the electrolyte phase is always zero.
As the reaction progresses from reactants to products by one molar extent, $\xi$, the Gibbs free energy of reaction may be related to the electrochemical potential of the reactants and products.
$\Delta G_R \equiv \frac{\partial G}{\partial \xi}\Big|_{T,P} = \sum_j \nu_j \mu_j$ 7
The electrochemical potential is a function of the species activity, $a_j$, and its Gibbs free energy of formation.
$\mu_j \equiv \frac{\partial G}{\partial N_j}\Big|_{T,P} = \Delta G^{\theta}_{f,j} + RT\ln(a_j) + z_j F\phi$ 8
By substitution and recalling previous electroneutrality arguments
$\Delta G_R = \Delta G^{\theta}_R + RT\sum_j \nu_j \ln(a_j) + nF(\phi_{electron} - \phi_{ion})\ ;\ \Delta G^{\theta}_R = \sum_j \nu_j \Delta G^{\theta}_{f,j}$ 9
At equilibrium, the Gibbs free energy of reaction will be zero and we can derive the Nernst equation for the equilibrium potential of the reduction reaction, $E^{red}_{eq}$.
$E^{red}_{eq} \equiv (\phi_e - \phi_i)_{eq} = E^{red}_0 - \frac{RT}{nF}\sum_j \nu_j \ln(a_j)\ ;\ E^{red}_0 = -\frac{\Delta G^{\theta}_R}{nF}$ 10
1 Bibliography


Electrochemistry Modeling for
Energy Conversion and Storage
SIEMENS
Ingenuity for life
Dr. C Lueth, Dr. C Walchshofer, Dr. V. Palaniasamy
Description
Theory
Results
Conclusions

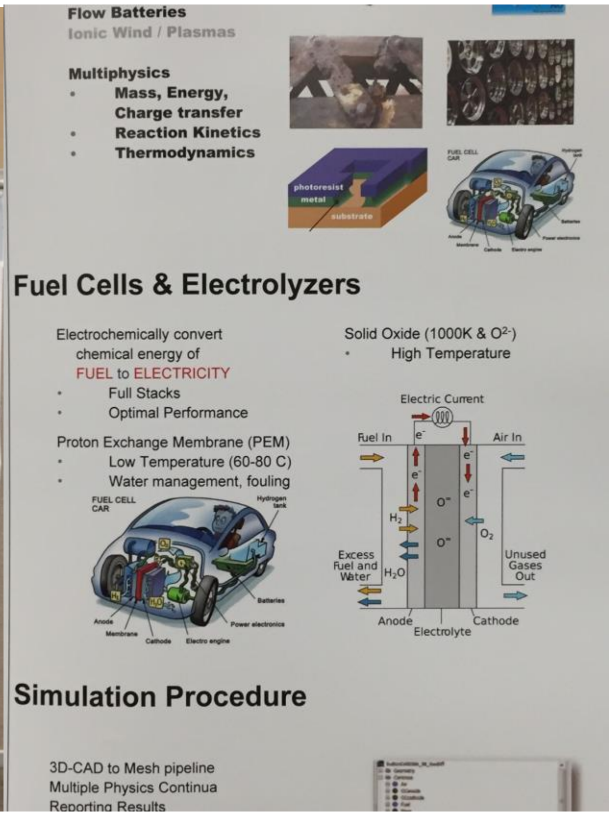
Flow Batteries
Ionic Wind / Plasmas
Multiphysics
Mass, Energy,
Charge transfer
Reaction Kinetics
Thermodynamics
photoresist
metal
substrate
Fuel Cells & Electrolyzers
Electrochemically convert
chemical energy of
FUEL to ELECTRICITY
Full Stacks
Optimal Performance
Proton Exchange Membrane (PEM)
Low Temperature (60-80 C)
Water management, fouling
Solid Oxide (1000K & O2-)
High Temperature
Electric Current
Fuel In
Air In
Excess Fuel and Water
Unused Gases Out
Anode
Electrolyte
Cathode
FUEL CELL CAR
Hydrogen tank
Batteries
Power electronics
Anode
Membrane
Cathode
Electro engine
Simulation Procedure
3D-CAD to Mesh pipeline
Multiple Physics Continua
Reporting Results

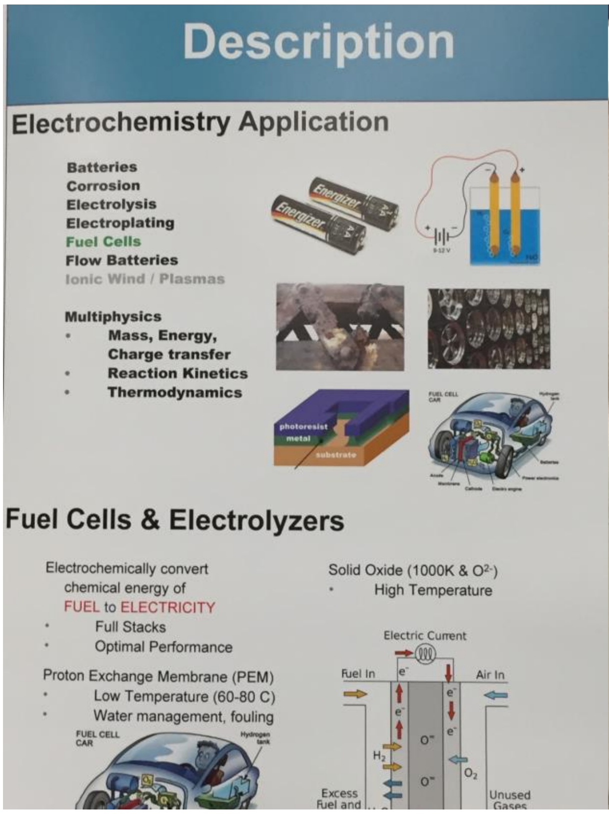
Description
Electrochemistry Application
Batteries
Corrosion
Electrolysis
Electroplating
Fuel Cells
Flow Batteries
Ionic Wind / Plasmas
Energizer
Multiphysics
Mass, Energy,
Charge transfer
Reaction Kinetics
Thermodynamics
photoresist
metal
substrate
Fuel Cells & Electrolyzers
Electrochemically convert
chemical energy of
FUEL to ELECTRICITY
Full Stacks
Optimal Performance
Proton Exchange Membrane (PEM)
Low Temperature (60-80 C)
Water management, fouling
Solid Oxide (1000K & O2-)
High Temperature
Electric Current
Fuel In
Air In

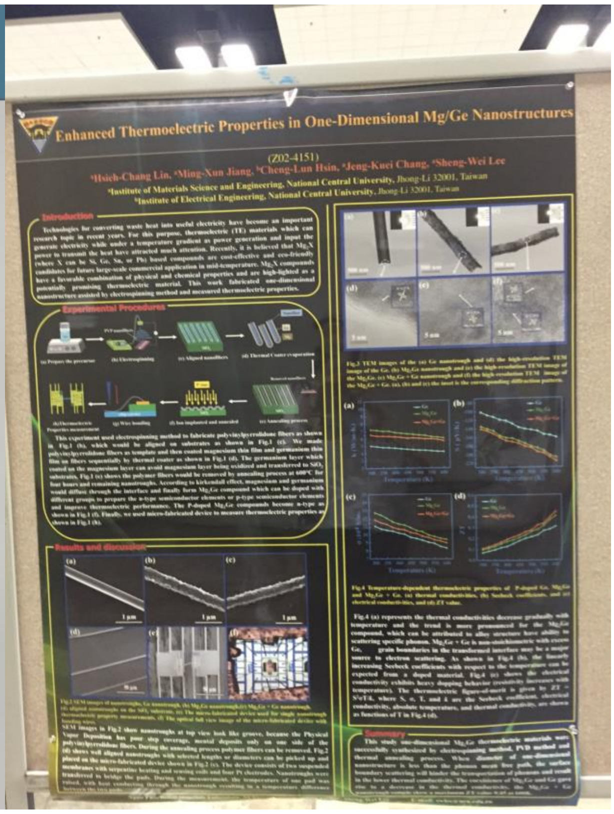
Enhanced Thermoelectric Properties in One-Dimensional Mg/Ge Nanostructures
(Z02-4151)
Introduction
Experimental Procedures
Results and discussion
Summary

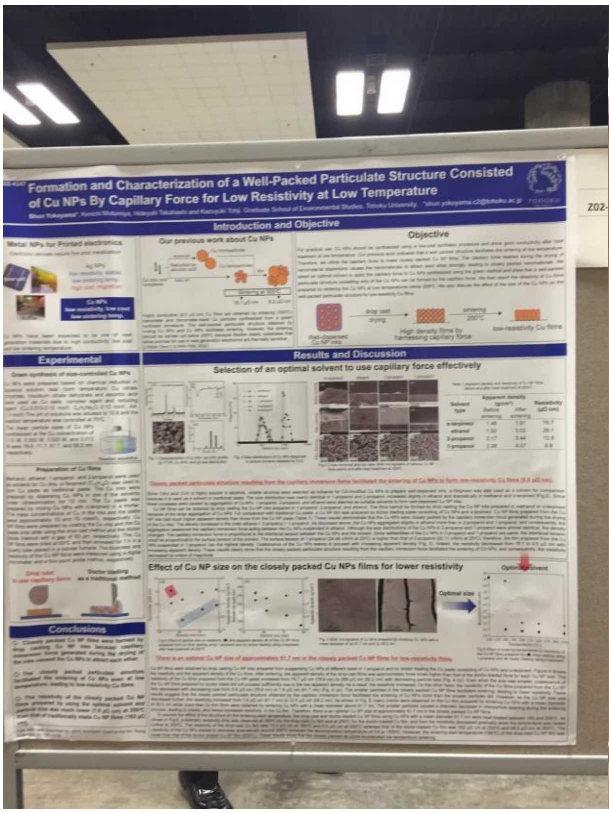
Formation and Characterization of a Well-Packed Particulate Structure Consisted of Cu NPs By Capillary Force for Low Resistivity at Low Temperature
Introduction and Objective
Objective
Experimental
Results and Discussion
Selection of an optimal solvent to use capillary force effectively
Effect of Cu NP size on the closely packed Cu NPs films for lower resistivity
Conclusions

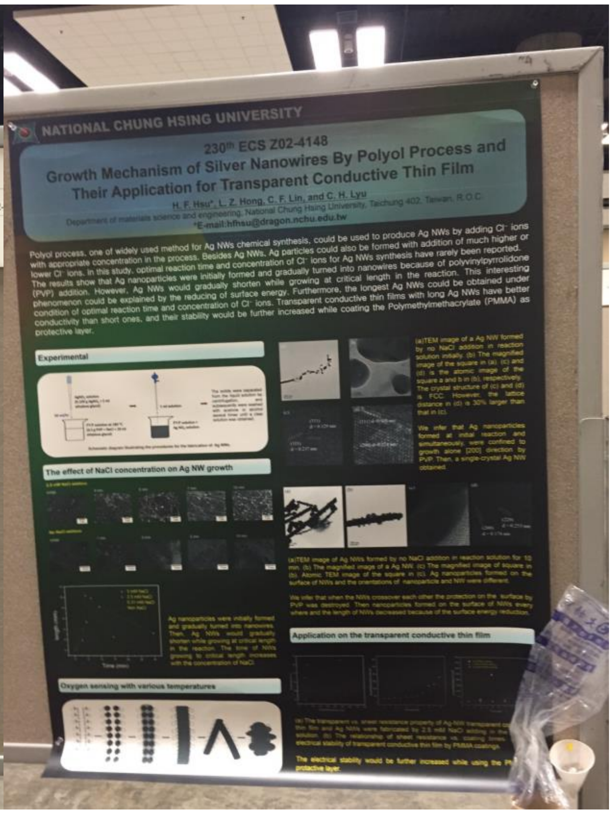
NATIONAL CHUNG HSING UNIVERSITY
230th ECS Z02-4148
Growth Mechanism of Silver Nanowires By Polyol Process and Their Application for Transparent Conductive Thin Film
Experimental
The effect of NaCl concentration on Ag NW growth
Oxygen sensing with various temperatures
Application on the transparent conductive thin film

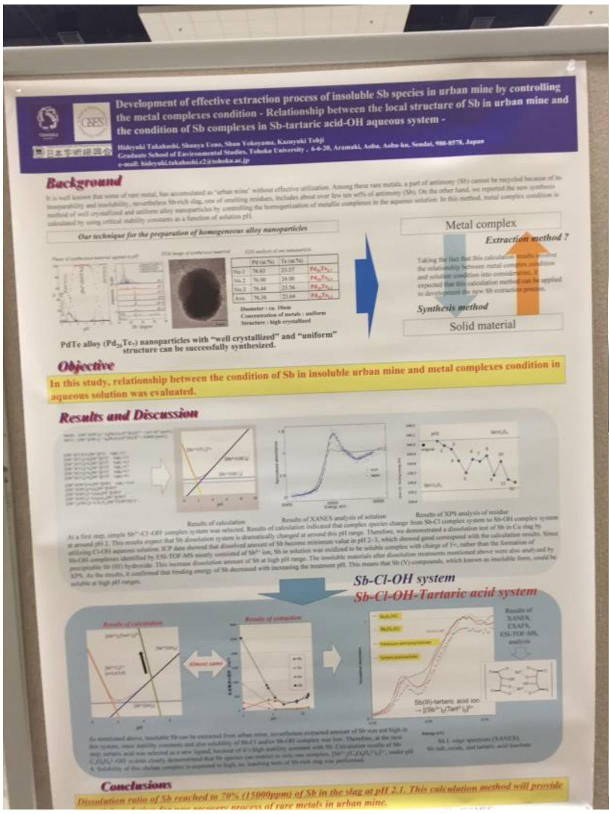
Development of effective extraction process of insoluble Sb species in urban mine by controlling the metal complexes condition - Relationship between the local structure of Sb in urban mine and the condition of Sb complexes in Sb-tartaric acid-OH aqueous system -
Background
Our technique for the preparation of homogeneous alloy nanoparticles
Metal complex
Extraction method ?
Synthesis method
Solid material
Objective
In this study, relationship between the condition of Sb in insoluble urban mine and metal complexes condition in aqueous solution was evaluated.
Results and Discussion
Sb-Cl-OH system
Sb-Cl-OH-Tartaric acid system
Conclusions

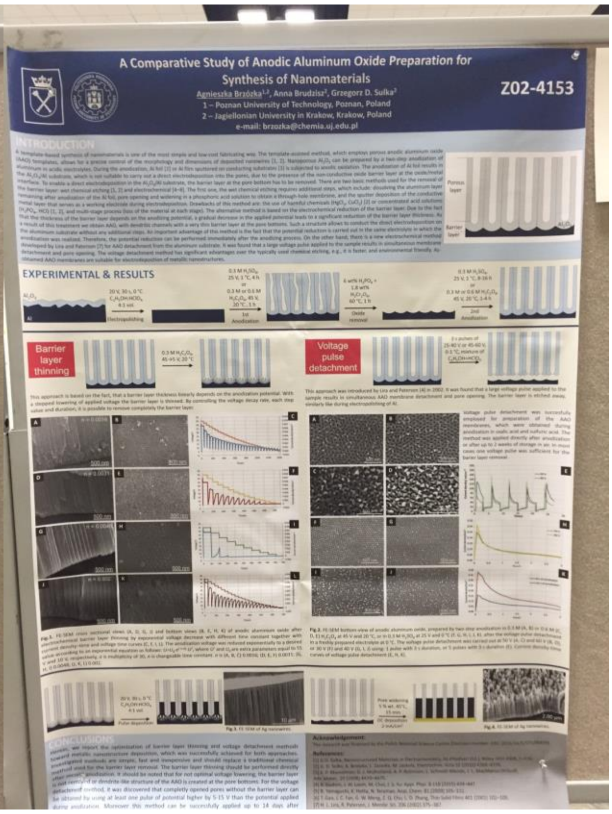
A Comparative Study of Anodic Aluminum Oxide Preparation for Synthesis of Nanomaterials
Z02-4153
Agnieszka Brzózka, Anna Brudzisz, Grzegorz D. Sulka
1 – Poznan University of Technology, Poznan, Poland
2 – Jagiellonian University in Krakow, Krakow, Poland
INTRODUCTION
EXPERIMENTAL & RESULTS
Barrier layer thinning
Voltage pulse detachment
CONCLUSIONS

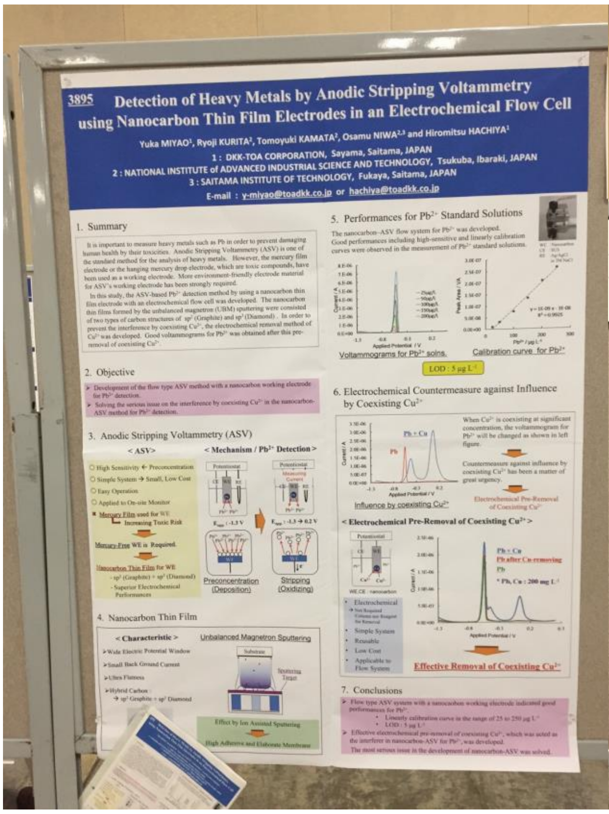
3895 Detection of Heavy Metals by Anodic Stripping Voltammetry using Nanocarbon Thin Film Electrodes in an Electrochemical Flow Cell
Yuka MIYAO1, Ryoji KURITA2, Tomoyuki KAMATA2, Osamu NIWA2,3 and Hiromitsu HACHIYA1
1 : DKK-TOA CORPORATION, Sayama, Saitama, JAPAN
2 : NATIONAL INSTITUTE of ADVANCED INDUSTRIAL SCIENCE AND TECHNOLOGY, Tsukuba, Ibaraki, JAPAN
3 : SAITAMA INSTITUTE OF TECHNOLOGY, Fukaya, Saitama, JAPAN
E-mail : y-miyao@toadkk.co.jp or hachiya@toadkk.co.jp
1. Summary
2. Objective
3. Anodic Stripping Voltammetry (ASV)
4. Nanocarbon Thin Film
5. Performances for Pb2+ Standard Solutions
6. Electrochemical Countermeasure against Influence by Coexisting Cu2+
7. Conclusions
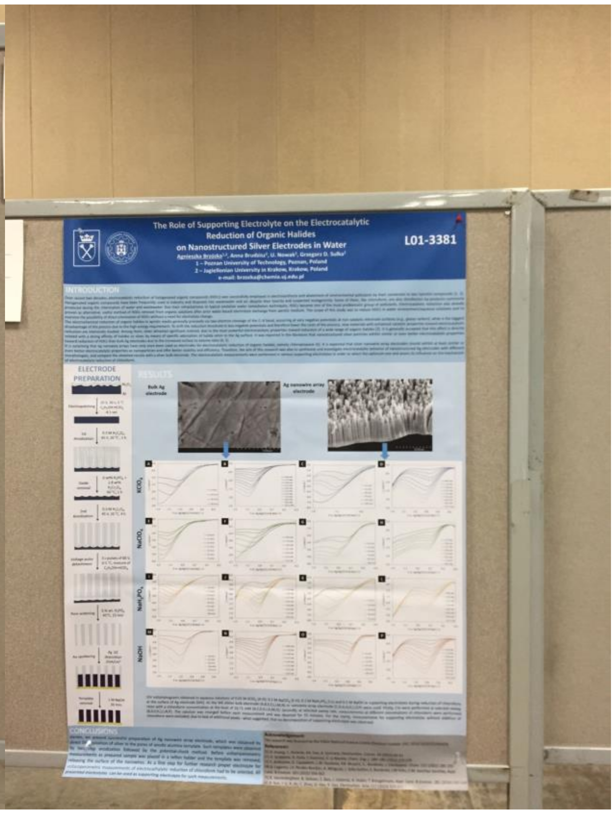
The Role of Supporting Electrolyte on the Electrocatalytic Reduction of Organic Halides on Nanostructured Silver Electrodes in Water
L01-3381
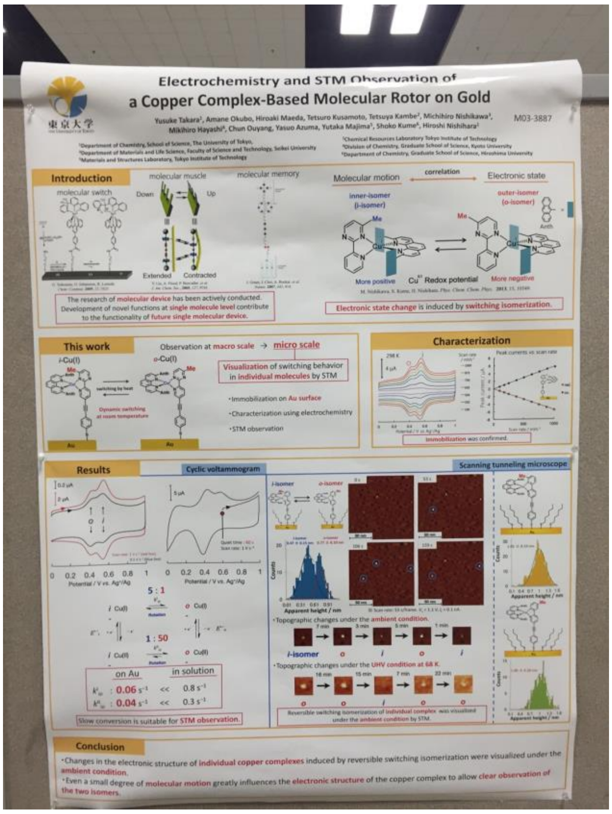
Electrochemistry and STM Observation of a Copper Complex-Based Molecular Rotor on Gold
M03-3887
Introduction
This work
Characterization
Results
Cyclic voltammogram
Scanning tunneling microscope
Conclusion

**The Effect of Thermal Hydrogenation Processing on the Nano-Size Grain Refinement and Oxide Layer Formation of Ti-6Al-4V Alloy**

L. M. Wang, C. J. Tsai

Chung Cheng Institute of Technology,
Dept. of Power Vehicle and System Engineering
University of National Defense, Taiwan, R.O.C.

# Introduction

1. Ti-6-4 alloy is a promising material.
   Major applications are in：
   - aerospace,
   - automobile,
   - military industries

   because of its ：
   - low density,
   - excellent mechanical,
   - corrosion properties

2/57

2. Recently, extensive studies have been reported on refinement of the grain size of titanium alloys using a thermohydrogenation process (THP) by employing hydrogen as a temporary alloying element.

   *THP, by using：
   hydrogenation and dehydrogenation process
   [Yu,06;She,07;She,09].


3/57

5. THP can produce nano grains.
   [Yu,06;She,07;She,09].

6. Oxide layer produced on nano grains may be a good way to enhance the corrosion resistance of Ti-6-4 alloy.

7. There are limited reports on the corrosion behavior of grain-refined Ti alloys resulting from the THP.

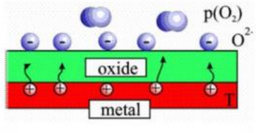


4/57

8. Control of $O_2$ flowing rate into the furnace containing THP processed sample of Ti-6-4 alloy may be possible to control the desirable thickness and composition of Ti-6-4 and therefore：
   improve the corrosion resistance of T-6-4 alloy.


5/57

The thickness of oxide layer and its corrosion resistance ($i_{corr}$) from related treatments vs. Earlier works in Literature

| References/ present work | Treatment Process | Electrolyte Solution | Thickness of Oxide Layer (μm) | $i_{corr}$ ($A/cm^2$) |
|---|---|---|---|---|
| Kumar et al.[20] | CP-Ti + heat-treatment (650°C /8~48 h) | Ringer's solution | 3.5~19 | $4.2 \times 10^{-7}$~$6.7 \times 10^{-6}$ |
| Kumar et al.[21] | CP-Ti + heat-treatment (500~800°C /24 h) | Ringer's solution | ~30 | $2.9 \times 10^{-7}$~$2.2 \times 10^{-5}$ |
| Kumar et al.[22] | Ti-6Al-4 V + heat-treatment (500~800°C /8~48 h) | Ringer's solution | 7~79 | $1.3 \times 10^{-8}$~$2.8 \times 10^{-7}$ |
| present work | Ti-6Al-4 V + BST + THP + ANN (704°C /2 h) | $H_2SO_4$ | 0.56 | $2.78 \times 10^{-10}$ |
| Present work | Ti-6Al-4 V + BST + THP + ANN($O_2$) (704°C /2 h + 50cc/min oxygen) | $H_2SO_4$ | 1.04 | $8.39 \times 10^{-11}$ |

Wang et al. , J. ECS, 160,(11) C560-C568(2013)

6/57

**However, in the literature:**

- **It is noted that the employed temperature for THP is mostly among the range of 650-850 ˚C with the amount of hydrogenation mostly lower than 0.4 H/M（the mole ratio of hydrogen to the alloy atoms of related alloy)**
  [Sun,09 ; Sha,07; Sha,08 ; Liu,09 ; Zhu,09 ; Zha,10; Zha,08;Sun,09; Li,07; Zon,07]

7/57

- **Yu [Yu,06] and Shen [She,14;She,09 ] studied THP at 600 ˚C with hydrogenation loading at the ranges 0.1-0.9 H/M and reported with disagreements in hydride formation and microstructure evolution with above reports.**

8/57

•Although the grain refinement in THP process was found as early as in 1979 by Mahajan et al. [Mah,79], the possible mechanism was not explained until in 2009 by Shen et al.[She,09] on the loading of 0.7 H/M at 600 ˚C in THP process, in which phase transformation was proposed as the main reason for the grain refinement.

9/57

• In 2010 Zhao et al.[Zha, 10] confirmed the phase transformation leading to the grain refinement and further proposed that the recrystallization may result in the grain refinement when studied THP with hydrogenation loading at 0.1-0.4 H/M at 750˚C and dehydrogenation at 700˚C.

• Shen et al. [she, 14]proposed that during hydrogenation process, the precipitation of the hydride of $\beta_H$ and δ phase leads to the defects in the matrix and these defects would be the main routes to cause the grain refinement.

10/57

•However, based on the phase diagram not in agreement and microstructure from SEM only possibly makes the uncertainty remained; as far as the defect is concerned, the lack of the atomic size scale evidence may lead to the different arguments.

•Thus, the phase diagram, microstructure evolution, the influence of produced defects to the grain refinement still need further studied to build up its more accurate features during THP process.

11/57

• The aim of this study is to add more understanding of the defect produced during THP process in terms of microstructure evolution leading to grain refinement with hydrogenation loading at 0.1-0.7 H/M at 600˚C and dehydrogenation at 600˚C.


12/57

# Experimental work

**Sample preparation**

- as-received(AR)
- β-solution treatment at 1050℃ in vacuum for 0.5 h, followed by furnace cooling to room temperature(AR+BST)

13/57

**THP treatment**

- Sievert's volumetric apparatus was used for THP treatment.
- Hydrogenation : 600 ℃/30 min
- Dehydrogenation : 600 ℃/2 h, followed by air cooling for approximately 30 min to room temperature.

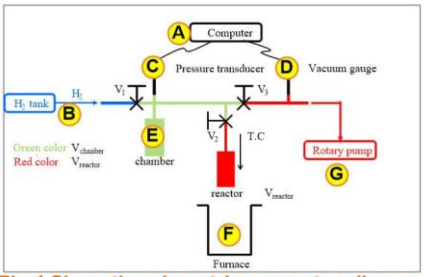


Fig.1 Sievert's volumetric apparatus diagram

14/57

**Annealing treatment**

- ANN : without $O_2$+Ar (500cc/min) at 704℃/2h/air cooling
- ANN plus $O_2$ : with $O_2$(50cc/min)+Ar (500cc/min) at 704℃/2h/air cooling

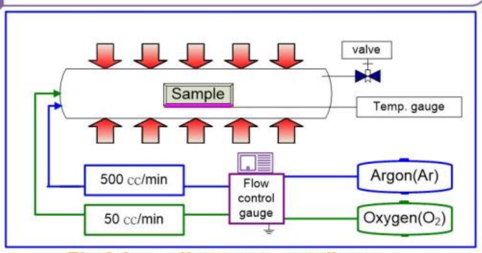


Fig.2 Annealing treatment diagram

All the samples were ground with SiC abrasive papers and further polished with fine grade diamond paste before each stage treatment.

15/57

# Result and Discussion

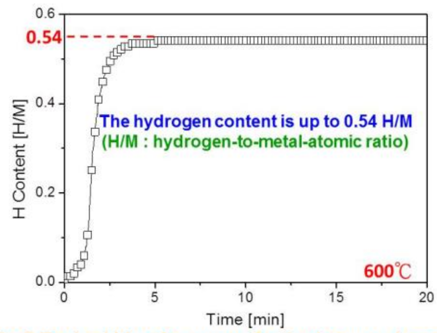


Fig.3 Typical kinetic curves for hydrogen absorption

16/57

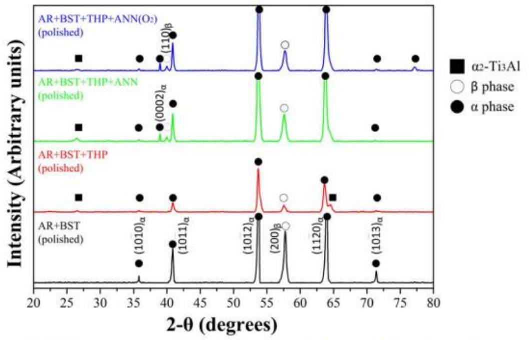


Fig.4 XRD patterns of Ti-6-4 alloy after related treatments. The identified phases of α, α2, and β are marked.

17/57

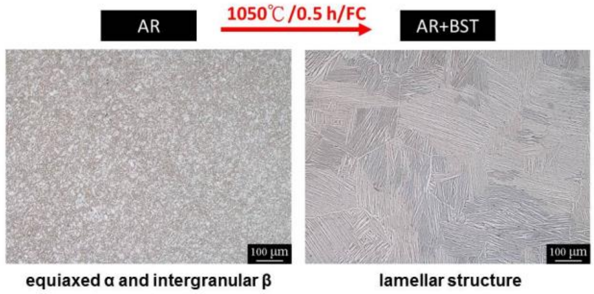


Fig.5 Optical micrographs of β-solution treated Ti-6-4 alloy

18/57

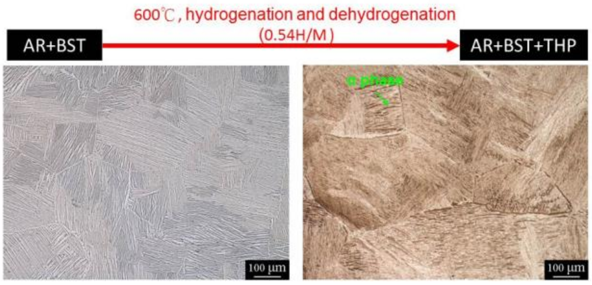


Fig.6 Optical micrographs of Ti-6-4 alloy subjected to THP treatment at 600℃ following β-solution treatment

the lamellar structure is preserved associated with severely etched feature after THP treatment

19/57

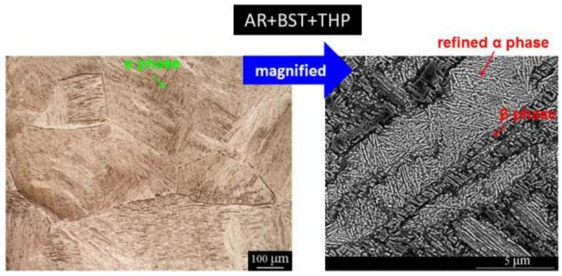


OM SEM

Fig.7 Optical and SEM micrographs of Ti-6-4 alloy subjected to THP treatment at 600℃

grain refinement within the α matrix is observed through SEM technique

20/57

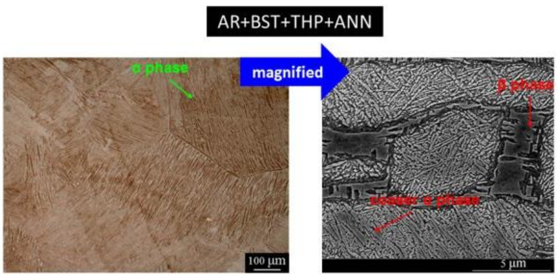


OM SEM

Fig.8 Optical and SEM micrographs of Ti-6-4 alloy subjected to post-THP annealing treatment (704℃/2h/air cooling)

the thicker α grains are obtained due to the effect of grain growth attributed by post-THP annealing treatment

21/57

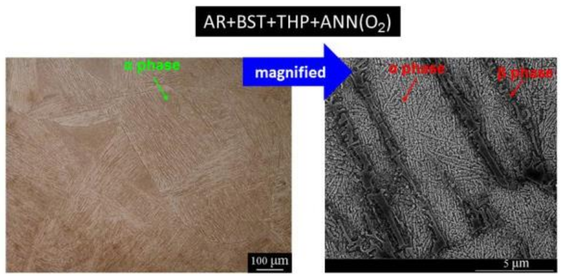


OM SEM

Fig.9 Optical and SEM micrographs of Ti-6-4 alloy subjected to post-THP annealing treatment with $O_2$

22/57

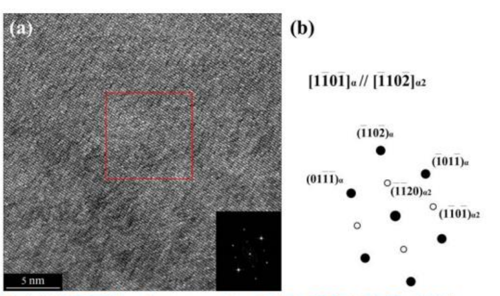


Fig.10 (a) HRTEM micrograph of AR+BST+THP+ANN condition and its Fast Fourier Transform analysis of the framed area inserted
(b) the corresponding schematic illustration of FFT pattern

23/57

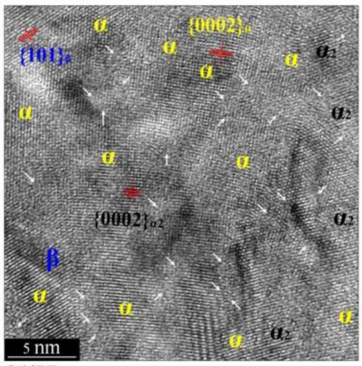


24/57

Fig.11

Relatively distorted region close to grain boundary are arrowed.

24/57

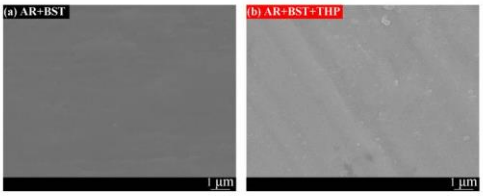


Fig.12 SEM micrographs of the top surface of oxidized Ti-6-4 alloy of AR+BST and AR+BST+THP conditions

*All the samples were ground with SiC abrasive papers and further polished with fine grade diamond paste before each stage treatment.

25/57

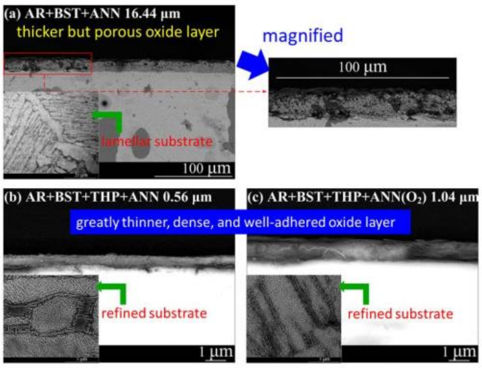


Fig.14 Cross sectional SEM micrographs of oxidized Ti-6-4 alloy after related treatments

Refined Ti-6-4 substrate producing thinner oxide layer

26/57

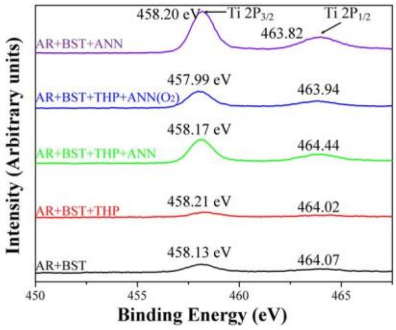


Fig.15 XPS spectra of the Ti 2p region of the top surface after related treatments

The Ti $2P_{3/2}$ peak was positioned at about 458.2 eV, indicating oxidized $Ti^{4+}$ in the form of $TiO_2$ in agreement with the work of Wang et al.(JMR, Vol. 24, No.12, pp3680-3688,2009)

27/57

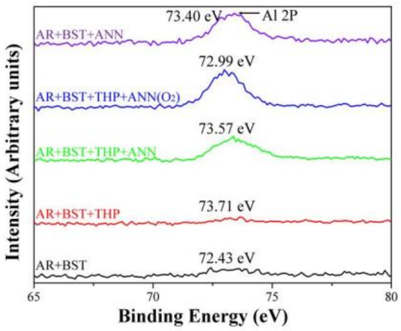


Fig.16 XPS spectra of the V 2p region of the top surface after related treatments

The Al 2P peak was positioned at about 73.2 eV, indicating oxidized $Al^{3+}$ in the form of $Al_2O_3$ in agreement with the work of Wang et al.(JMR, Vol. 24, No.12, pp3680-3688,2009)

28/57

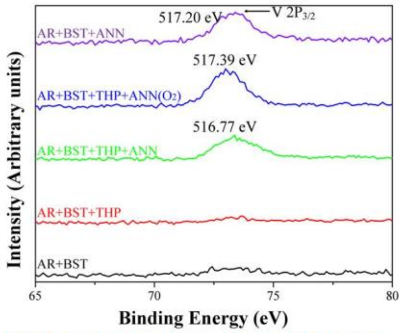


Fig.17 XPS spectra of the V 2p region of the top surface after related treatments

The V 2P peak was positioned at about 516.9 eV, indicating oxidized $V^{5+}$ in the form of $V_2O_5$ in agreement with the work of Wang et al.(JMR, Vol. 24, No.12, pp3680-3688,2009)

29/57

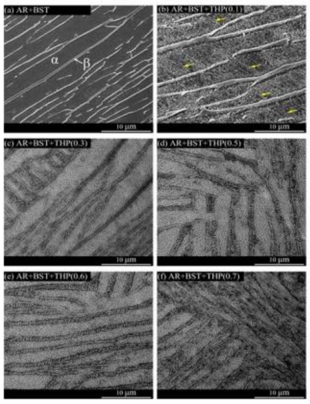


Fig.18

SEM image after related hydrogen loadings (0.1-0.7 H/M)

30/57

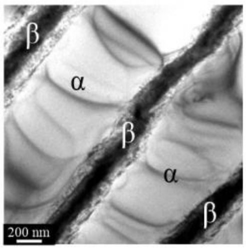


Fig.19

Typical parallel alpha and Beta structures

31/57

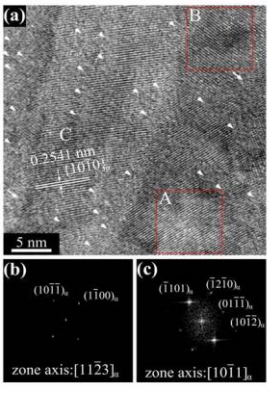


Fig.20

Ti-6Al-4V THP loading 0.1 H/M

32/57

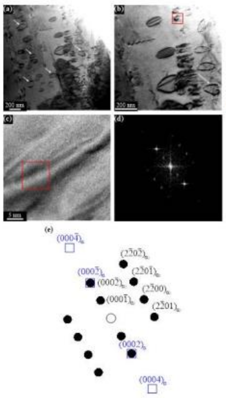

( Ti-6Al-4V THP loading 0.1 H/M)

Fig.21 Dislocation loops together with Delta phase being detected

33/57

Fig.22

Ti-6Al-4V THP loading 0.3 H/M

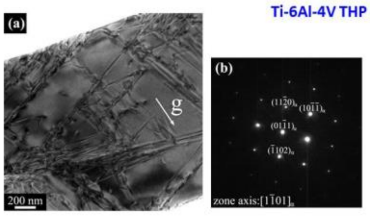

34/57

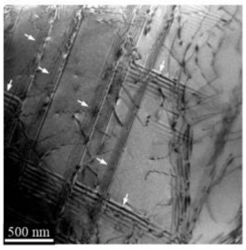

Fig.23

(Ti-6Al-4V THP loading 0.3 H/M)

Stacking faults as arrowed in TEM.

35/57

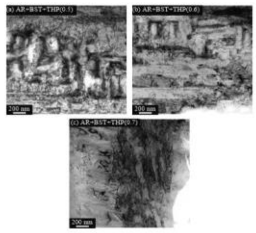

Fig.24

Ti-6Al-4V THP loading 0.5, 0.6, 0.7 H/M

36/57

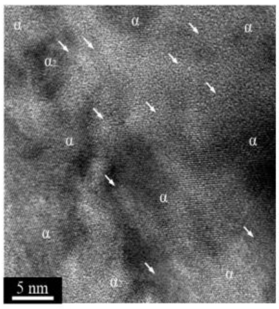

Fig.25

Ill defined area as arrowed in the HRTEM image

(Loading at 0.7 H/M)

37/57

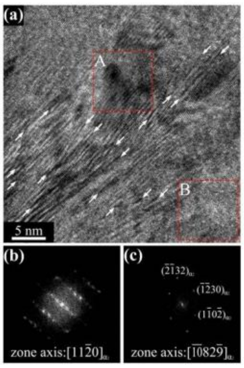

Fig.26

Stacking faults as arrowed in matrix are observed loading at 0.7H/M )

38/57

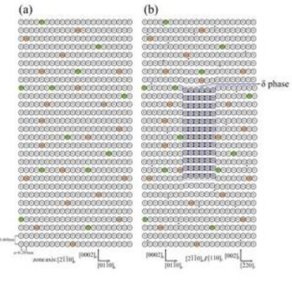

Fig.27

**After THP, possible mechanism of dislocation loop formation and stacking fault produced.**

39/57

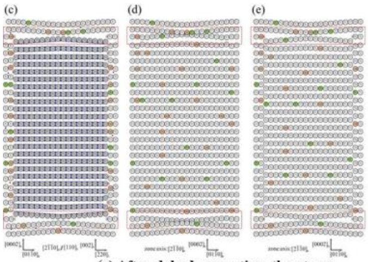

(e) After dehydrogenation, the atoms arrangements of delta phase inversely transformed to alpha phase.

The schematic model proposed to illustrate the found dislocation loop and the remained stacking faults in matrix.;

(d) is not easy to occur since the significant strain energy may be increased.

Fig.28

40/57

Fig.29

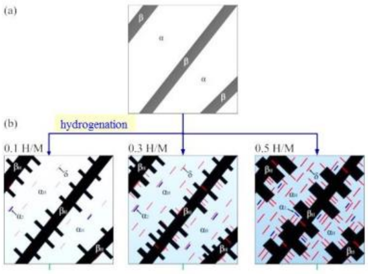


(a) The α+β lamellar structure after β solution treatment,
(b) After 0.1, 0.3 or 0.5 H/M THP hydrogenation the schematic microstructure evolutions

41/57

(c) After dehydrogenation, the δ phase inversely transformed to α + β phase, resulting in a grain refinement effect.

Fig.30

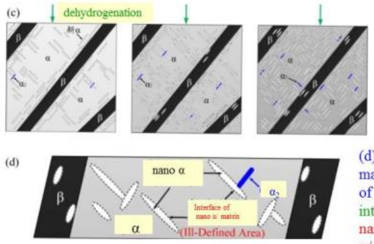


(d)The magnified image of (c); the interfaces of nano α/α , α/β or α/α$_2$ may form the ill-defined area.

42/57

The Ti, Al and V atoms in the ill defined area that may lead to the amorphous like microstructure.

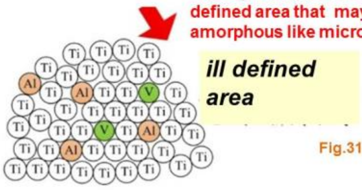


Fig.31

43/57

# Conclusions

- The THP process results in the formation of refinement structures (refinement of α matrix by breaking it into several pieces) and the precipitation of $\alpha_2$ ($Ti_3Al$) in Ti-6-4 alloy.

44/57

- Ill defined areas present the amorphous characterics that can form an area to cut the continuity of the lattice arrangements ; as a result, nano α, precipitate of nano $\alpha_2$ can form refined α and β and this blocking effect can result in a grain refinement.

45/57

## References


[Sun,09] Sun, Z., Hou, H., Zhou, W., Wang, Y., and Li, Z., "The Effect of Hydrogen on Microstructures Evolution and Deformation Behaviors of Ti-6Al-4V Alloys," *Journal of Alloys and Compounds*, Vol. 476, pp. 550-555, 2009.

[Sha,07] Shan, D. B., Zong, Y. Y., Lu, T. F., and Lv, Y., "Microstructural Evolution and Formation Mechanism of FCC Titanium Hydride in Ti-6Al-4V-xH Alloys," *Journal of Alloys and Compounds*, Vol. 427, pp. 229-234, 2007.


46/57


[Sha,08] Shan, D. B., Zong, Y. Y., Lv, Y., and Guo, B., "The Effect of Hydrogen on the Strengthening and Softening of Ti-6Al-4V Alloy," *Scripta Materialia*, Vol. 58, pp. 449-452, 2008.

[Liu,09] Liu, H. J., Zhou, L., Liu, P., and Liu, Q. W., "Microstructural Evolution and Hydride Precipitation Mechanism in Hydrogenated Ti-6Al-4V Alloy," *International Journal of Hydrogen Energy*, Vol. 34, pp. 9596-9602, 2009.

[Zhu,09] Zhu, T. and Li, M., "Effect of 0.770 wt.% H Addition on the Microstructure of Ti-6Al-4V Alloy and Mechanism of δ Hydride Formation," *Journal of Alloys and Compounds*, Vol. 481, pp. 480-485, 2009.


47/57


[Zha,10] Zhao, J., Ding, H., Zhong, Y., and Lee, C. S., "Effect of Thermo Hydrogen Treatment on Lattice Defects and Microstructure Refinement of Ti6Al4V Alloy," *International Journal of Hydrogen Energy*, Vol. 35, pp. 6448-6454, 2010.

[Zha,08] Zhao, J. W., Ding, H., Zhao, W. J., Tian, X. F., Hou, H. L., and Wang, Y. Q., "Influence of Hydrogenation on Microstructures and Microhardness of Ti6Al4V Alloy," *Transactions of Nonferrous Metals Society of China*, Vol. 18, pp. 506-511, 2008

[Sun,09] Sun, Z., Zhou, W., and Hou, H., "Strengthening of Ti-6Al-4V Alloys by Thermohydrogen Processing," *International Journal of Hydrogen Energy*, Vol. 34, pp. 1971-1976, 2009.


48/57

[Li,07] Li, M. and Lin, Y., "Grain Refinement in near Alpha Ti60 Titanium Alloy by the Thermohydrogenation Treatment," *International Journal of Hydrogen Energy*, Vol. 32, pp. 626-629, 2007.

[Zon,07] Zong, Y. Y., Shan, D. B., Lü, Y., and Guo, B., "Effect of 0.3 wt.% H Addition on the High Temperature Deformation Behaviors of Ti-6Al-4V Alloy," *International Journal of Hydrogen Energy*, Vol. 32, pp. 3936-3940, 2007.

49/57

[Yu,06] Yu, C. Y., Shen, C. C., and Perng, T. P., "Microstructure of Ti-6Al-4V Processed by Hydrogenation," *Scripta Materialia*, Vol. 55, pp. 1023-1026, 2006.

[She,14]Shen, C. C. and Wang, C. M., "Effects of Hydrogen Loading and Type of Titanium Hydride on Grain Refinement and Mechanical Properties of Ti-6Al-4V," *Journal of Alloys and Compounds*, Vol. 601, pp. 274-279, 2014.

50/57

[She, 09] Shen, C. C., Yu, C. Y., and Perng, T. P., "Variation of Structure and Mechanical Properties of Ti-6Al-4V with Isothermal Hydrogenation Treatment," *Acta Materialia*, Vol. 57, pp. 868-874, 2009.

[Mah,79]Mahajan, Y., Nadiv, S., and Kerr, W. R., "Studies of Hydrogenation in Ti-6Al-4V Alloy," *Scripta Metallurgica*, Vol. 13, pp. 695-699, 1979.

51/57

**Thanks for**

**your attention**

52/57